A TRIDENT SCHOLAR PROJECT REPORT

NO. 245

THE INFLUENCE OF CRYSTAL ORIENTATION ON THE CORROSION BEHAVIOR OF ALUMINUM

UNITED STATES NAVAL ACADEMY
ANNAPOLIS, MARYLAND

REPORT DOCUMENTATION PAGE

Form Approved
OMB No. 074-0188

1. AGENCY USE ONLY (Leave blank)	2. REPORT DATE	3. REPORT TYPE AND DATE COVERED
	7 May 1997	

4. TITLE AND SUBTITLE
The influence of crystal orientation on the corrosion behavior of aluminum

5. FUNDING NUMBERS

6. AUTHOR(S)
Brandon W. Davis

7. PERFORMING ORGANIZATION NAME(S) AND ADDRESS(ES)
U.S. Naval Academy
Annapolis, MD

8. PERFORMING ORGANIZATION REPORT NUMBER
USNA Trident Scholar project report no. 245 (1997)

9. SPONSORING/MONITORING AGENCY NAME(S) AND ADDRESS(ES)

10. SPONSORING/MONITORING AGENCY REPORT NUMBER

11. SUPPLEMENTARY NOTES
Accepted by the U.S. Trident Scholar Committee

12a. DISTRIBUTION/AVAILABILITY STATEMENT
This document has been approved for public release; its distribution is UNLIMITED.

12b. DISTRIBUTION CODE

13. ABSTRACT: Observations have been made which indicate that the pitting of aluminum is crystallographic. When pure aluminum pits, the resulting morphology of the pit is composed of (100) orientations. Metastable and stable pitting was examined for (100), (110), and (111) aluminum single crystals and polycrystalline aluminum with 99.99% purity. Evidence was seen that the (111) orientation had a higher affinity for initiation and propagation and the (100) orientation had the least affinity for these mechanisms. Also, there was evidence that suggested that the hydrogen cathodic kinetics on the single crystal orientations increased in the following order: (100), (110), (111). It is suggested that the crystallographic pitting of aluminum is due to these differences in electrochemical reaction rates. Specifically, the (100) and (111) crystal orientations corrode at a faster rate, leaving behind a (100) morphology within the pit.

14. SUBJECT TERMS
Aluminum, Anisotropy, Corrosion, Crystallography, Pitting

15. NUMBER OF PAGES

16. PRICE CODE

17. SECURITY CLASSIFICATION OF REPORT	18. SECURITY CLASSIFICATION OF THIS PAGE	19. SECURITY CLASSIFICATION OF ABSTRACT	20. LIMITATION OF ABSTRACT

U.S.N.A. --- Trident Scholar project report; no. 245 (1997)

THE INFLUENCE OF CRYSTAL ORIENTATION ON THE CORROSION BEHAVIOR OF ALUMINUM

by

Midshipman Brandon W. Davis, Class of 1997
United States Naval Academy
Annapolis, Maryland

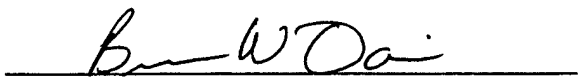

Certification of Adviser Approval

Professor Patrick J. Moran
Department of Mechanical Engineering

7 May 1997

Acceptance for the Trident Scholar Committee

Professor Joyce E. Shade
Chair, Trident Scholar Committee

7 May 97

ABSTRACT

Observations have been made which indicate that the pitting of aluminum is crystallographic. When pure aluminum pits, the resulting morphology of the pit is composed of (100) orientations. Metastable and stable pitting was examined for (100), (110), and (111) aluminum single crystals and polycrystalline aluminum with 99.999% purity. Evidence was seen that the (111) orientation had a higher affinity for initiation and propagation and the (100) orientation had the least affinity for these mechanisms. Also, there was evidence that suggested that the hydrogen cathodic kinetics on the single crystal orientations increased in the following order: (100), (110), (111). It is suggested that the crystallographic pitting of aluminum is due to these differences in electrochemical reaction rates. Specifically, the (110) and (111) crystal orientations corrode at a faster rate leaving behind a (100) morphology within the pit.

KEYWORDS: Aluminum, Anisotropy, Corrosion, Crystallography, Pitting

TABLE OF CONTENTS

NOMENCLATURE

1. **Ecorr:** Corrosion potential
2. **Epass:** Passivation potential
3. **Epit:** Pitting potential
4. **Erp:** Repassivation potential
5. **Ipass:** Passive Current Density
6. **NRL:** Naval Research Laboratory
7. **SCE:** Saturated calomel electrode
8. **USNA:** United States Naval Academy

INTRODUCTION

Aluminum is a metal that is widely used throughout the Navy. Its applications include aircraft components as well as the superstructures on ships such as the Ticonderoga Class Cruiser. The advantage of using aluminum as a material derives from its properties. Specifically, aluminum's low density makes it a favorable choice for applications requiring a light weight and high strength material. Additionally, aluminum has an excellent resistance to uniform corrosion.

Although aluminum has excellent uniform corrosion resistance, it has a large affinity for localized corrosion in the presence of chloride and other halide ions. Localized corrosion occurs when discrete sites on the surface begin to corrode, while the remainder of the surface remains passive and unattacked. Specifically, aluminum is subject to a form of localized corrosion called pitting. Pitting is a dangerous form of corrosion because it can lead to failure with a relatively small amount of material. Generally, corrosion is measured in total amount of material lost. With pitting, only a small amount of total material

is lost. If this material were spread evenly across the entire surface, the corrosion would not be a problem. However, since the corrosion occurs in an accelerated manner at discrete sites, perforation or other failure can compromise the integrity of the material. Not only is localized corrosion potentially dangerous, but its random nature makes it difficult to control or to provide allowances for during engineering design.

It has been found that when pure aluminum pits, it does so in an anisotropic manner. An anisotropic material is one that does not have the same properties in all directions throughout its crystal structure. Specifically, the pitting of aluminum is dependent on crystal orientation. Examinations of the pits have shown that the resulting crystal orientation during pitting is the (100) orientation within the pit. The crystallography of aluminum will be described in the Background Section.

There were four main objectives to this project. The first objective was to determine the extent of metastable pitting, pits that form but do not propagate, as a function of crystal orientation. Metastable pitting occurs below the pitting potential. The pitting potential is the critical

potential at which stable pitting initiates. The second objective was to quantify the influence of crystallographic orientation on the pitting potential of aluminum. The third objective was to understand why (100) facets develop when aluminum pits. Work on the first three objectives led to the fourth objective, which was to contribute to a better understanding of the faceted pitting of aluminum based on the electrochemical properties of the individual crystallographic orientations.

This research has great importance in the area of corrosion resistance. An understanding of the corrosion resistance of each crystal orientation might lead to alloy chemistries that enable aluminum alloys to have an increased corrosion resistance. Additionally, advanced processing techniques could be developed that utilize the different corrosion properties of the crystal orientations. These advanced processing techniques would involve producing a material whose surface orientations are entirely composed of the higher corrosion resistant orientation. Lastly, inhibitors might be designed to limit the corrosion of other crystallographic facets based on the corrosion process of the (100) orientation.

BACKGROUND

CRYSTAL STRUCTURE OF ALUMINUM

Since the different crystal orientations in aluminum behave in different manners, it is important to understand the crystal nature of aluminum. Aluminum has a face centered cubic unit cell structure. The unit cell is a small unit that describes the pattern to which aluminum atoms arrange themselves. Additionally the unit cell is a small volume that shows all of the structural characteristics of the system. This means that the unit cell has the same properties as the crystal.

Aluminum's unit cell is referred to as face centered cubic because the center of an atom is at the center of each side of the cubic unit cell. Additionally, face centered cubic crystals have an atom at each corner of the unit cell (Figure 1). Within this unit cell, there are three major planar orientations. These three orientations are called the (100), (110), and (111) crystal plane orientations. The location of these three orientations with respect to the unit cell is shown in Figure 2. The different crystal orientations also have different atomic arrangements. These

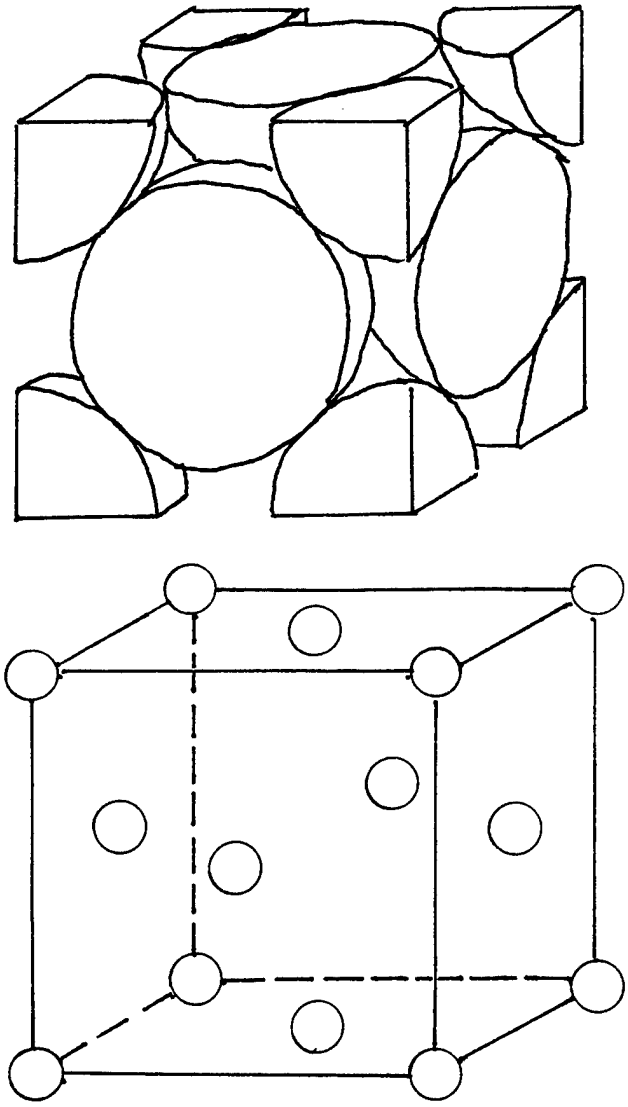

FIGURE 1: The arrangement of atoms in an aluminum unit cell, which is face centered cubic.

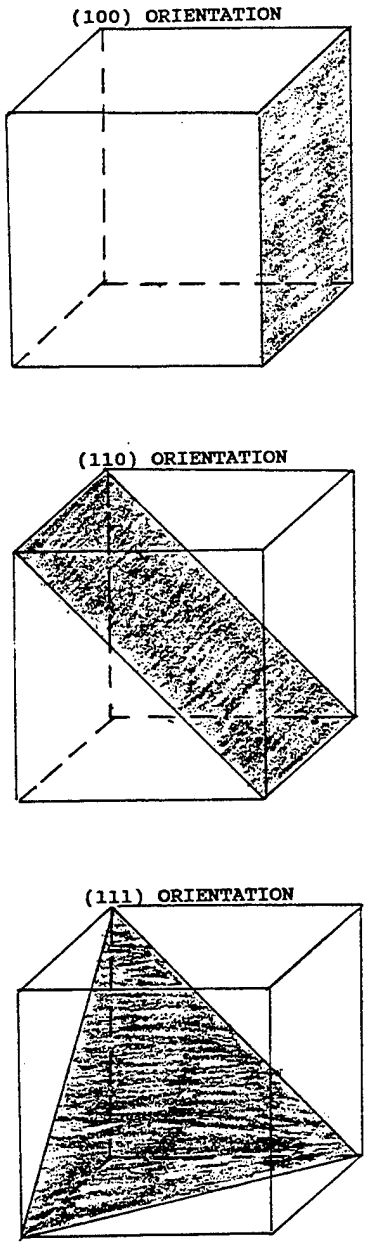

FIGURE 2: Location of the (100), (110), and (111) crystal orientations in an aluminum unit cell.

arrangements and the respective dimensions of the unit cell are shown in Figure 3. Often the differences in the atomic arrangements of the crystal orientations lead to differences in the properties of the crystal orientations.

Corrosion is a complex process that is affected by numerous factors. Because of this complexity, it is advantageous to study metals in their simplest form. This form would be as a single crystal. A single crystal is defined as a crystal that has the same atomic relationship and orientation throughout its entire structure. In a single crystal, each unit cell is oriented in the same direction and same plane. In contrast, a polycrystalline material contains multiple crystals, or grains. At locations called grain boundaries, which are the boundaries of the individual crystals, the orientation of the unit cells change. Often, materials have different properties across grain boundaries. Nevertheless, the single crystal can be used to examine the basic behavior of the metal as influenced by the crystal orientation.

Anisotropic behavior refers to an element that does not have the same properties throughout its structure. Specifically, crystallographic anisotropy means that one

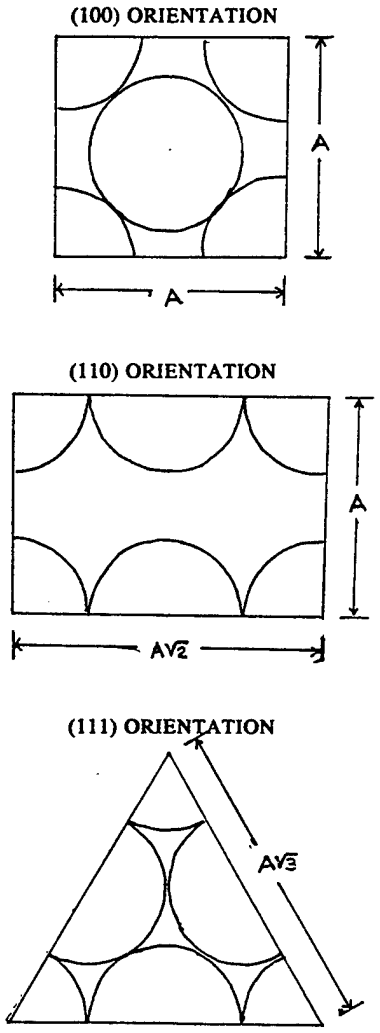

FIGURE 3: Atomic arrangement of the three crystal orientations for aluminum.

crystal orientation reacts differently than another crystal orientation. While it is possible to study crystallographic anisotropy using polycrystalline materials, this requires the grain boundaries to be identified and a single grain to be isolated. It is much easier to isolate a crystal orientation using a monocrystalline material. Orem demonstrated that the monocrystalline disk was the best geometric form to utilize to study the effect of crystal orientation on the corrosion rate [1].

GENERAL CORROSION BEHAVIOR OF ALUMINUM

An important aspect of aluminum is the fact that it is thermodynamically unstable in its natural state. Because of this instability, aluminum quickly reverts back to its stable form which is an aluminum oxide. This transition to stability is achieved through corrosion. As the aluminum begins to corrode and become more stable, it produces aluminum ions which react with the environment to form aluminum oxides as a corrosion product that collect on the surface. These oxides quickly produce a thin film on the surface of the aluminum. This protective oxide barrier bonds to the surface of aluminum and restricts the ability

of uniform corrosion to occur. On a freshly abraded surface that is exposed to air, the oxide layer can be as thin as 1 nanometer thick, yet it is effective in resisting the further corrosion of the aluminum. This oxide layer's protection is termed passivity. Passivity occurs if, on increasing a metal's potential to more positive values, the rate of corrosion does not accelerate.

The aluminum oxide barrier that forms is not stable under all conditions. The conditions for the stability of the oxide film are expressed by a Pourbaix diagram (Figure 4). As shown in the diagram, the oxide barrier protects aluminum (passivation) in a pH range of about 4 to 8.5. These values vary somewhat with temperature, the specific form of oxide film, and with the presence of substances that form soluble complexes or insoluble salts with aluminum. At a pH above and below the passivation range, aluminum corrodes in aqueous solutions because its oxides are soluble.

Even in the passive region of the Pourbaix Diagram, aluminum exhibits corrosion, mainly in the form of localized corrosion. Localized corrosion in the passive range occurs when the protective oxide barrier fails at a discrete site.

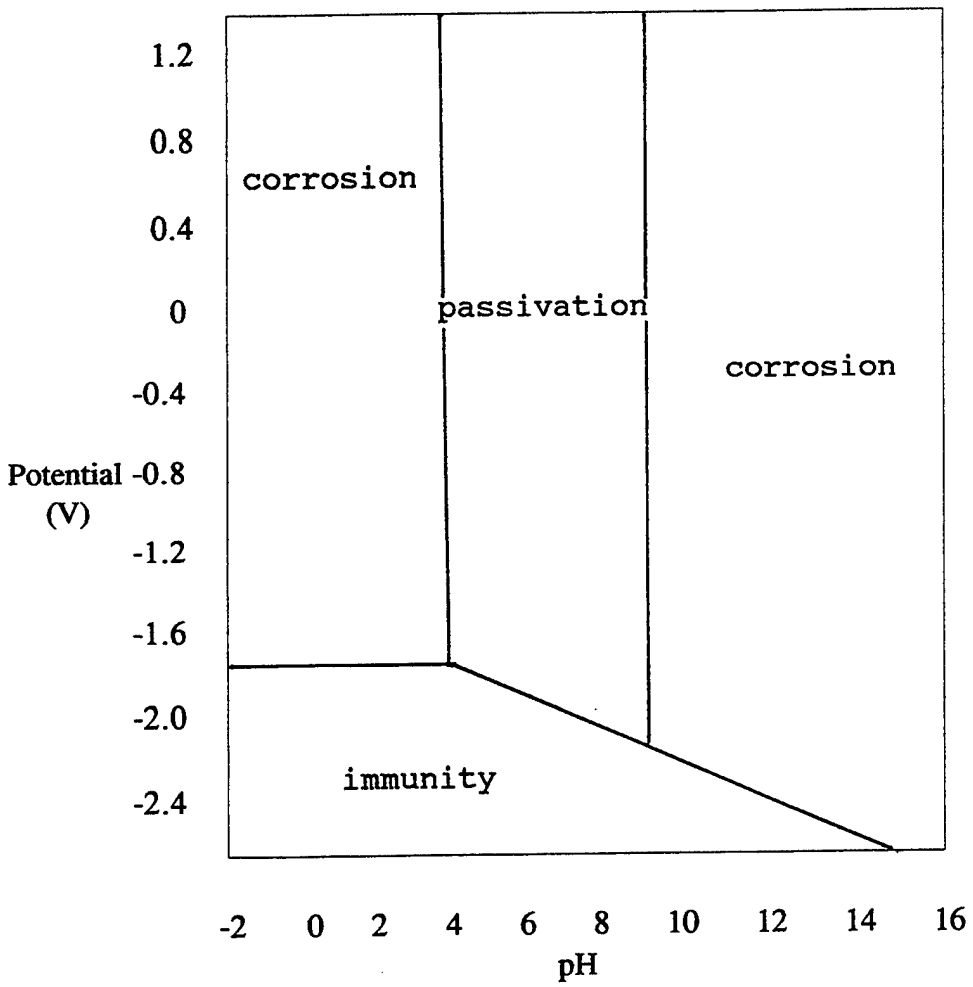

FIGURE 4: The Pourbaix diagram of aluminum. This diagram shows the behavior of aluminum at given potentials and pH levels.

This breakdown generally occurs at discontinuities in the oxide layer. Along with the discontinuities, an aggressive species is usually required to help break down the barrier. This aggressive species is usually chloride ions, which are readily abundant in marine environments.

In a neutral pH environment, the phenomenology of the active-passive behavior of a metal is best shown by a polarization curve (Figure 5). A polarization curve is generated during a potentiodynamic scan, which plots the electrochemical potential versus the log of the current density for a metal. The electrochemical potential of a metal can be established in one of three different ways. The potential could be established by the reaction of the metal with the environment. An example of this is the oxidation of aluminum. The second method of establishing a potential is with a galvanic couple with another metal where the natural potentials of two metals are pulled together through their contact. The last method of establishing a potential is through electrically forcing the potential of the metal in either the positive or negative direction. In the polarization curve, the current density is linearly proportional to the corrosion rate, meaning that as the

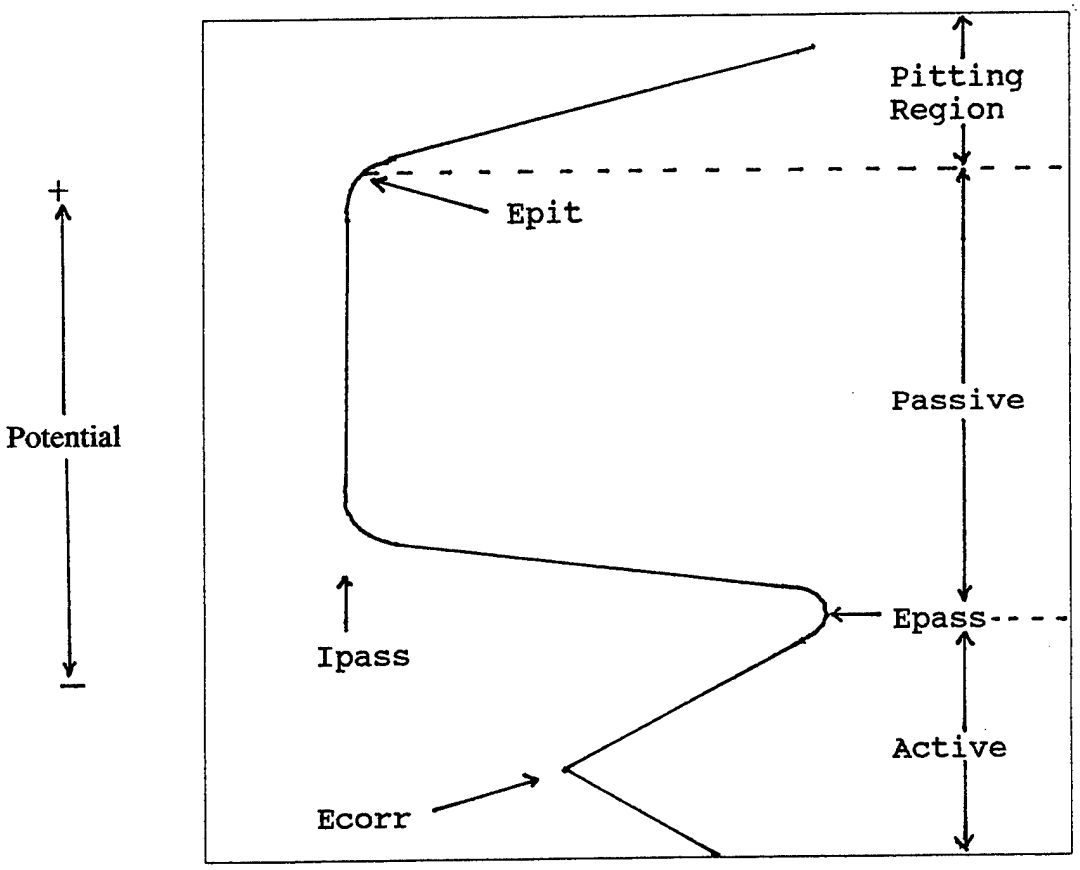

FIGURE 5: The polarization curve of an active-passive metal. A polarization curve is generated with a potentiodynamic scan.

current density increases, the amount of metal that is corroding increases. Because of the relationship, the polarization curve shows the rate of corrosion as a function of electrochemical potential.

An examination of the polarization curve shows that as the curve begins at the lowest potential and proceeds to higher potentials, the current density decreases as the potential increases. The first important potential found on the polarization curve is the corrosion potential (Ecorr). The corrosion potential is the natural potential of a metal in its environment. The corrosion potential occurs at the point where the current density transitions from decreasing to increasing levels as the potential is increased. This transition is caused by the intersection of the anodic and cathodic reaction curves of the metal, i.e. where the oxidation rate (anodic) equals the reduction rate (cathodic). The anodic reaction curve is the curve which plots the rate of metal dissolution as a function of electrochemical potential. The cathodic reaction curve is the curve which plots the reaction by which a species such as oxygen or hydrogen ions is reduced. Corrosion occurs where these two reaction rates are equal because the

electrons released in the pit (anodic reaction) have to be consumed by the cathodic reaction reactant, usually hydrogen ions.

As the potential increases above the corrosion potential, the current density continues to increase. This region, where the current density is increasing, is termed the active region. Aluminum's polarization curve (Figure 6) does not exhibit this active region because of the presence of its natural oxide film. This oxide film maintains aluminum's passivity, thereby restricting the appearance of the active region nose. Even if the aluminum oxide layer was absent from the surface, the hydrogen reaction of aluminum would still hide the active nose. Once the potential increases to a certain point called the passivation potential (Epass) on an active-passive metal, the current density quickly falls off to low passive values (Ipass). In this region, the film that has formed on the surface protects, or passivates, the surface. Again, in the case of aluminum, this passive oxide is already present, but thickens in the passive region. If this surface oxide layer is scratched or damaged, it will reform quickly in this region. The range of potentials for which the oxide layer

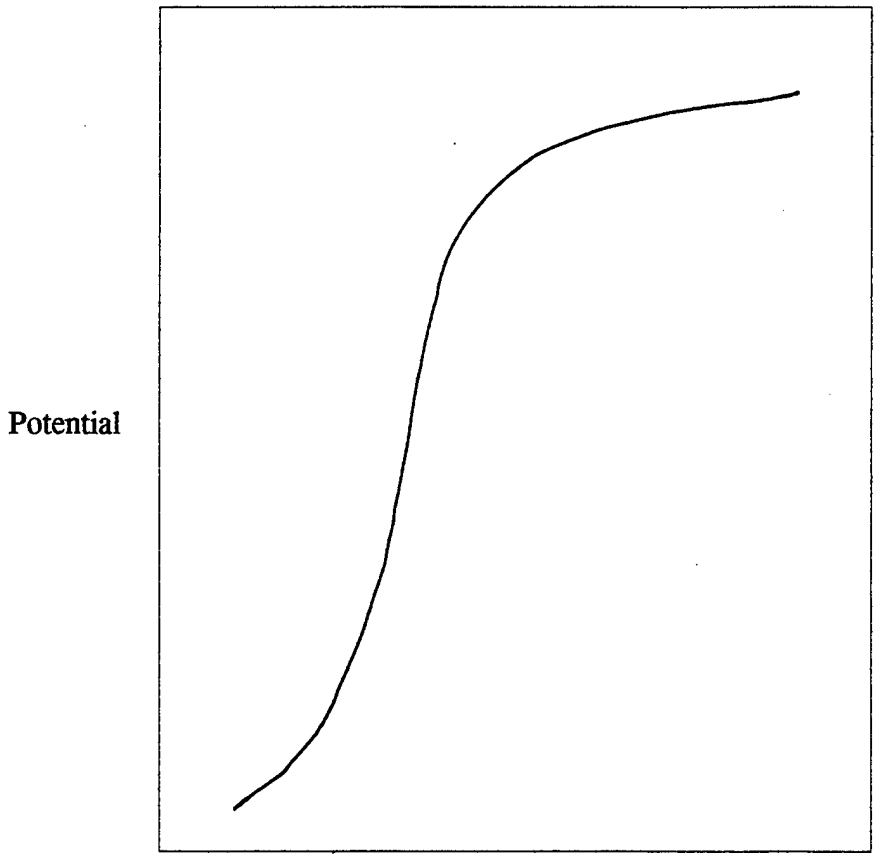

FIGURE 6: The polarization curve of aluminum. The active nose is missing because aluminum passivates due to its oxide film.

protects the surface is termed the passive region. As the potential is increased in the passive region, it will reach a critical potential at which the current density increases abruptly. This is called the pitting potential (Epit). At this potential, the passive film breaks down at discrete sites and the surface begins to pit. Above the pitting potential, the material experiences increasing levels of pitting damage to the surface. The region above the pitting potential is known as the pitting region.

If the potential of the aluminum is lowered from the pitting region, after sufficient stable pitting has occurred, the current density decreases until it meets the initial passive current density line. Once the potential of the aluminum reaches the passive current density the pits have repassivated. This potential is known as the repassivation potential (Erp).

The pitting process can be broken down into two stages: initiation and propagation. Initiation occurs when the protective aluminum oxide surface is compromised and discrete sites of attack develop. Some of these sites will either reform the protective oxide layer, called repassivation of a metastable pit, or they will continue to

grow. When an initiated site continues to grow, propagation occurs, i.e. stable pitting. Propagation includes the following features: an aggressive pit solution, hydrogen gas evolution within the pit, and often blistering occurs when the gas evolution proceeds without the oxide barrier having been appreciably perforated [2].

It has been experimentally found that some pits form at potentials well below the pitting potential [3]. When pits initiate below Epit, the oxide layer usually reforms and the pits repassivate. This mechanism is termed metastable pitting. It has also been established that the frequency and intensity of metastable pitting increases as the potential approaches the pitting potential [3].

It has been proposed that the probability of stable pitting is directly linked to the occurrence and intensity of metastable pitting [3]. This leads to the idea that a study of metastable pitting will give insight into the mechanisms of pit formation, stabilization and growth. Little is understood about the actual mechanisms of metastable pitting. However, it is believed that the pit repassivates because it cannot maintain the critical pit chemistry required [4].

The chemistry of the solution within the pit is critical for the pitting process to persist. As the aluminum in the pit corrodes, hydrogen ions are generated in the pit during the hydrolysis reaction caused by the buildup of aluminum ions. The hydrogen ions acidify the solution within the pit. Because of the nature of the pit and its depth, the diffusion of the hydrogen ions to the bulk solution is restricted. Hence, once the pit chemistry becomes acidic enough, the pitting continues and the pit maintains the acidity. The presence of an acidic pit chemistry is a necessity for pit growth since it prevents repassivation of the pit walls. When the pit is not able to maintain the aggressive chemistry, the pit will stop propagating and will repassivate.

Extensive tests have been conducted to determine the pH of the solution within a pit [4]. Because of the fact that there will always be some mixing between the pit solution and the bulk solution, the actual pit chemistry will not be able to maintain the theoretical pit chemistry. The theoretical pit chemistry is reported to have a pH between 3 and 4 [4,5]. Because of the intermixing of the pit chemistry with the bulk solution, the actual pit chemistry

is reported to have a pH of around 5.5 [4].

As the pit propagates, the hydrolysis reaction results in a local pH reduction within the pit. The effect of this pH reduction is an autocatalytic mechanism for pit propagation because low pH environments do not allow the passive oxide film to reform and this accelerates the rate of pitting. The propagation of aluminum pits have been shown to have anisotropic behavior [6,7]. This behavior will be discussed in the next section.

PAST WORK ON THE ANISOTROPIC CORROSION OF ALUMINUM

The pitting potential has been examined as a function of the exposed crystal orientation for aluminum. Yasuda et al. discovered that the pitting potential is dependent on the surface orientation [8]. They found that the pitting potential of the surface orientations follow the order: Epit (001) > Epit (011) > Epit (111). Their experiments included exposing 99.99% single aluminum crystals in 0.5M NaCl. The pitting potential for the (100), (110), and (111) orientation were found to be -700mV vs SCE, -724mV vs SCE, and -739mV vs SCE respectively. SCE refers to the saturated calomel reference electrode used as a reference in the

experiments. These values were the average of at least five separate experiments.

A good correlation has been found such that as the pitting potential of a material becomes more positive, the corrosion resistance of the material increases [9]. Based on this knowledge and the work of Yasuda et al. on the pitting potential of single crystal aluminum, the order of corrosion resistance of single crystal aluminum is, in increasing order, (111), (110), (100).

While it has been found that the pitting potential is dependent on the crystal orientation, it has been found that the surface orientation has no effect on the repassivation potential of pure aluminum single crystals [8]. These repassivation experiments were conducted on 99.99% pure aluminum in 0.5 M NaCl. The repassivation potential was found to be -800mV vs SCE for all three orientations. This experiment could be complicated by the fact that the pitting is crystallographic. Since all pits have walls that are (100) orientations, the repassivation of the pits would only be dependent on the rate of repassivation of the (100) orientation and this may be the reason for all three orientations having the same repassivation potential.

There are three major areas in which the anisotropic propagation of aluminum has been examined. These three areas are the pit morphology existing after stable pitting has occurred, the pit density of the different orientations, and the rate of pitting of the different orientations. The first of these major areas, pit morphology involves the resulting orientations in a pit. Experiments have shown that the morphology of all three crystal orientations after pitting exhibited only (100) orientation faces in the pit [6,7]. The (100) oriented crystal exhibited rectangular pits whose bottoms were parallel to the crystal surface. The (110) oriented crystal showed V shaped pits. Lastly, the (111) oriented crystals showed pits that had a regular tetrahedron shaped morphology with one point down. The morphology of the (111) oriented crystal at the surface of was triangular. These experimental results showed that the (100) crystal orientation is the rate limiting orientation for the pitting of aluminum.

The second major area is the pitting density, i.e. number of pits per unit area, on the crystal surface. Yasuda et al found that the pitting density is dependent on the crystal orientation [8]. They pitted aluminum crystals

at constant current densities for 1000 seconds in 0.5 M sodium chloride solution. They found that the pitting density was 14 pits per square millimeter for the (100) crystal, 22 pits per square millimeter for the (110) crystal, and 43 pits per square millimeter for the (111) crystal. Together, these results showed that the density of pits in polycrystalline aluminum was in the following order (111)>(110)>(100). This also demonstrated that the (100) crystal had the highest corrosion resistance, while the (111) crystal had the least corrosion resistance.

The third major area of past work regarding the anisotropic behavior of the propagation of aluminum pits investigated the rate at which the pits in each orientation propagate. Arora and Metzger performed experiments measuring the rate of uniform corrosion for different orientations. These experiments were conducted in 16% HCl [7]. This test solution was much more concentrated than the solution that is thought to exist within pits. The form of aluminum that was used during the tests was polycrystalline aluminum. Single crystals were not isolated on the polycrystalline aluminum, rather the depth of corrosion was measured on each crystal orientation based against a

reference orientation. They found that the (111) orientation corroded 71% faster than the (100) orientation and the (110) orientation corroded 41% faster than the (100) orientation. These results showed that the corrosion propagation resistance is in the following increasing order (111), (110), (100).

While these results showed an obvious difference in the rate of corrosion of the different crystal orientations, there were some problems with the experimental procedure used for the tests. The polycrystalline aluminum used contained impurities such as iron and copper. These impurities could have influenced the rate of corrosion on the crystal orientations. Also, once a crystal orientation begins to corrode, (100) facets appear. The presence of these facets on each crystal orientation would make distinguishing the rate of corrosion for each orientation difficult and raises questions about the validity of the data.

EXPERIMENTAL PROCEDURES

SINGLE CRYSTALS OBTAINED FROM THE MONOCRYSTALS COMPANY

Aluminum single crystals of three different orientations were purchased from the Monocrystals Company located in Richmond Heights, Ohio. The three orientations purchased were (100), (110), and (111). The single crystals were 99.999% pure as feedstock prior to crystal growth. The aluminum crystals were obtained in rod form. The crystals were grown using the Bridgmann method. This method uses an aluminum seed crystal with a given orientation. Molten aluminum is poured into a mold on top of the seed crystal and allowed to slowly grow in the same orientation as the seed crystal. This results in an aluminum structure which has the same crystalline orientation throughout its structure. The mold used in growing the crystals was a graphite mold. The Laue diffraction method was used to obtain an accurate orientation of the crystals once they were grown. Once the orientation was obtained, the crystals were cut using a diamond abrasive saw to obtain the orientation desired. The crystals were cylindrically round; 0.5 inches in diameter and 2 mm thick after cutting.

The company then lapped and polished the crystals using progressively finer alumina or diamond polishers. Finally the crystals were polished with a coloidal silica. The mechanism used to polish the crystals was a precision machine fixture that contained a round plate fixture that was parallel to the polishing surface. The crystal were cemented onto the fixture and lowered onto the polishing surface. Once the polishing was completed, ethanol was used to remove the abrasive materials present on the crystal. The accuracy of the crystal orientation was guaranteed to within +/- 2 degrees with usually a one degree margin of error as the result. The orientations were confirmed using X-ray diffraction.

POLYCRYSTALLINE ALUMINUM SAMPLES

The polycrystalline aluminum samples were obtained from the Naval Research Laboratory. The polycrystalline aluminum was obtained in two forms. The first form was 99.99% pure aluminum in coupon form. These specimens were used to develop the experimental techniques that were subsequently used on the single crystals and on the 99.999% pure polycrystalline aluminum.

The second form of polycrystalline aluminum was 99.999% pure aluminum obtained in rod form. The rods were cut using a diamond abrasive saw into 3mm sections that were 0.625 inches in diameter.

SPECIMEN PREPARATION FOR THIS RESEARCH

Once the aluminum crystals were received, polishing was required for several reasons. First, the crystals were received with scratches on their surfaces. Polishing removes all scratches and existing pits that can lead to extraneous corrosion or noise in an experiment. Second, the single crystals were required to be polished so that the face of the crystal was entirely the same orientation. This could only be achieved if the crystal face was perfectly flat.

Polishing was conducted using a standard copper polishing wheel combined with a Buehler Ecomet II Polisher. A rubber covering was adhesively connected to the polishing wheel to prevent galvanic coupling from occurring between the crystal and the polishing wheel [10]. A polishing cloth was then adhesively attached to the rubber surface. The polishing cloths used were Buehler Mastertex polishing cloths for 8 inch polishing wheels.

The polishing cloths were then prepared for polishing by extensively wetting them with distilled water. Once the polishing cloth was saturated with water, the excess water was removed by placing pressure by hand on the center of the cloth and pressing outward. After the excess water was removed, a lubricant was applied to the polishing cloth. The lubricant used was Struers DP-lubricant blue. The lubricant was applied from a spray bottle. The spray bottle was sprayed ten times onto the polishing cloth so that there was sufficient lubricant on the cloth without excess. Natishan et al. found that excess water or lubricant on the polishing cloth increases the chances of producing an orange peel effect on the surface of the crystal [10]. After wetting and lubricating the cloth, the polishing material was applied to the polishing cloth.

The polishing process was completed in three different stages for expediency. Each stage coincided with a certain size polishing material. The first stage used a 6 micron diamond solution as the polishing material. This solution was Buehler Metadi Diamond Suspension. This initial polishing stage was used to remove all scratches as well as polishing out all preexisting pits. The second stage of

polishing involved improving the surface finish. A 3 micron diamond spray was used in the second stage. The 3 micron diamond spray used was Struers DP-Spray P. The final polishing stage produced a mirror-like finish on the surface of the crystal, ensuring that there were no surface defects present. A 1 micron diamond spray was used as the polisher in the final stage. The 1 micron diamond spray was Struers DP-Spray HQ. Between each stage, the polishing cloth was replaced, a new one prepared, and the crystal was rinsed with distilled water and ethanol. This was to ensure that there was no carry-over of the polishing material from the previous stage. If a 6 micrometer particle existed on the cloth when the second polishing stage was being performed, then the polishing would result in unwanted scratches.

The actual polishing was performed by hand. The hand-held crystal was slowly lowered onto the prepared polishing cloth and rotated against the rotation of the polishing wheel. Only the weight of the hand was used to place pressure on the crystal to ensure that the crystal surface remained flat against the polisher. In this manner, the orientation of the crystal face was maintained. The crystal was polished in this manner for no longer than 60

seconds at a time. Natishan et al found that polishing times longer than a minute could lead to the orange peel surface [10]. Between each polishing period the crystal was also rinsed with distilled water to remove excess particles and polishing debris. The polishing was completed once the crystal had been polished to a mirror-like finish without any visible surface defects present. A visual inspection was used to ensure that there were no large surface defects, while optical microscopy was used to ensure that the crystals were free of smaller surface defects.

After the crystals were polished and passed the inspection, they were cleaned. The crystals were first rinsed in acetone to remove any dirt or polishing debris that existed. The acetone was purchased from the J.T. Baker Chemical Company, having a minimum purity of 99.5%. Ethanol was then used as a rinsing agent to remove any other dirt particles as well as removing any acetone that was present on the surface of the crystal. The ethanol was dehydrated 200 proof and was purchased from Pharmco. Lastly, an air spray was used to evaporate the ethanol, ensuring that there were no spots, and removing any dust that had settled on the crystal face. The air spray was "Global Precision Dust

Remover". The air spray did not affect the surface finish since the particle size was filtered by the manufacturer to less than 0.2 microns. Once the cleaning was completed the crystals were ready for mounting. The preparation of the polycrystalline samples was performed in the same manner as the single crystals.

MOUNTING OF SPECIMEN

The initial method of mounting the crystals was to place them in a lollipop holder. This holder consisted of several parts. The crystal fit into a stainless steel cylinder. Into this cylinder was threaded a metallic rod. The crystal, the cylinder, and the rod all maintained electrical contact. A teflon piece was threaded into the back of the stainless steel cylinder so that the back of the crystal was not exposed to the solution. A teflon or rubber washer was placed on the face of the crystal in order to isolate the crystal face. The washer was pressed between the crystal and the teflon outer body of the lollipop holder exposing only the crystal face. Lastly, the rod was surrounded by a glass tube that was sealed against the teflon body. This tube insulated the rod from exposure to

the test solution.

An examination of the crystals after testing with the lollipop holder showed that considerable crevice corrosion had occurred. Crevice corrosion is a form of localized corrosion where a crevice is depleted of oxygen and it becomes anodic with respect to the metal surface outside of the crevice. The electrochemical data that was generated during these tests involved both pitting and crevice corrosion. The attributes of each form of localized corrosion could not be separated. Therefore, the crevice corrosion was masking the pitting results. Because of this problem, the lollipop holder was abandoned and a new method of mounting the crystals was used.

The new method of mounting the crystals involved mounting them to a scrap piece of aluminum that was connected to a metallic rod. Since electrical contact needed to be maintained through the rod and scrap aluminum to the crystal, the rod was threaded into the scrap aluminum. The rod and the scrap aluminum, with the exception of the face of the scrap aluminum, were insulated. The insulation needed to be added so that the only metallic surface exposed to the test solution was the polished

surface of the crystal. The rod was insulated by heat-shrinking plastic tubing around the rod. This plastic cover sealed the metallic rod from the environment. The sides and back of the scrap aluminum were insulated using a glyptal lacquer, as will be described below. The glyptal laquer used was Glyptal 1201 Red, a silicone based coating purchased from Glyptal Inc.

The aluminum crystals were then mounted to the scrap piece of aluminum using a carbon glue. The carbon glue used was a low resistance contact cement purchased from Ernest F Fullam. This carbon glue enabled the crystal to be attached to the scrap aluminum while maintaining electrical contact between the scrap aluminum and rod.

After the carbon glue had sealed the crystal to the scrap aluminum, all surfaces, except for part of the front face of the crystal, were isolated by applying glyptal, leaving only a small, predetermined amount of the crystal face exposed. The amount of area exposed to the environment was measured and recorded to standardize the results based on area. For the metastable tests mentioned below, it was important that the glyptal was applied so that there would be no crevice corrosion at the edges of the glyptal.

Because of this the glyptal was applied in three separate coats. For the Ecorr tests mentioned below, the glyptal was applied in only one coat. The extra two coats were not needed because the potential of the crystal was not electrically driven more positive and crevice corrosion was therefore not a problem. The extra two coats of glyptal were also not used for the HCl tests mentioned below because of the fact that crevice corrosion did not occur in the HCl solution. The glyptal was carefully applied to the crystal using a small paintbrush. The glyptal lacquer, applied as a liquid, had an extended curing time. Because of the importance of ensuring the glyptal was dry before testing, each coat of glyptal was allowed 48 hours of drying time at room temperature.

Once the last coat of glyptal had cured, the crystal was ready for testing. To ensure that the crystal surface was free of any debris, the air spray was used to remove any additional dust that had settled on the crystal face just before testing the crystal.

The electrochemical cell used for the testing was a Model K0047 Corrosion Cell Kit from EG&G Princeton Applied Research (Figure 7). The software used for the experiments

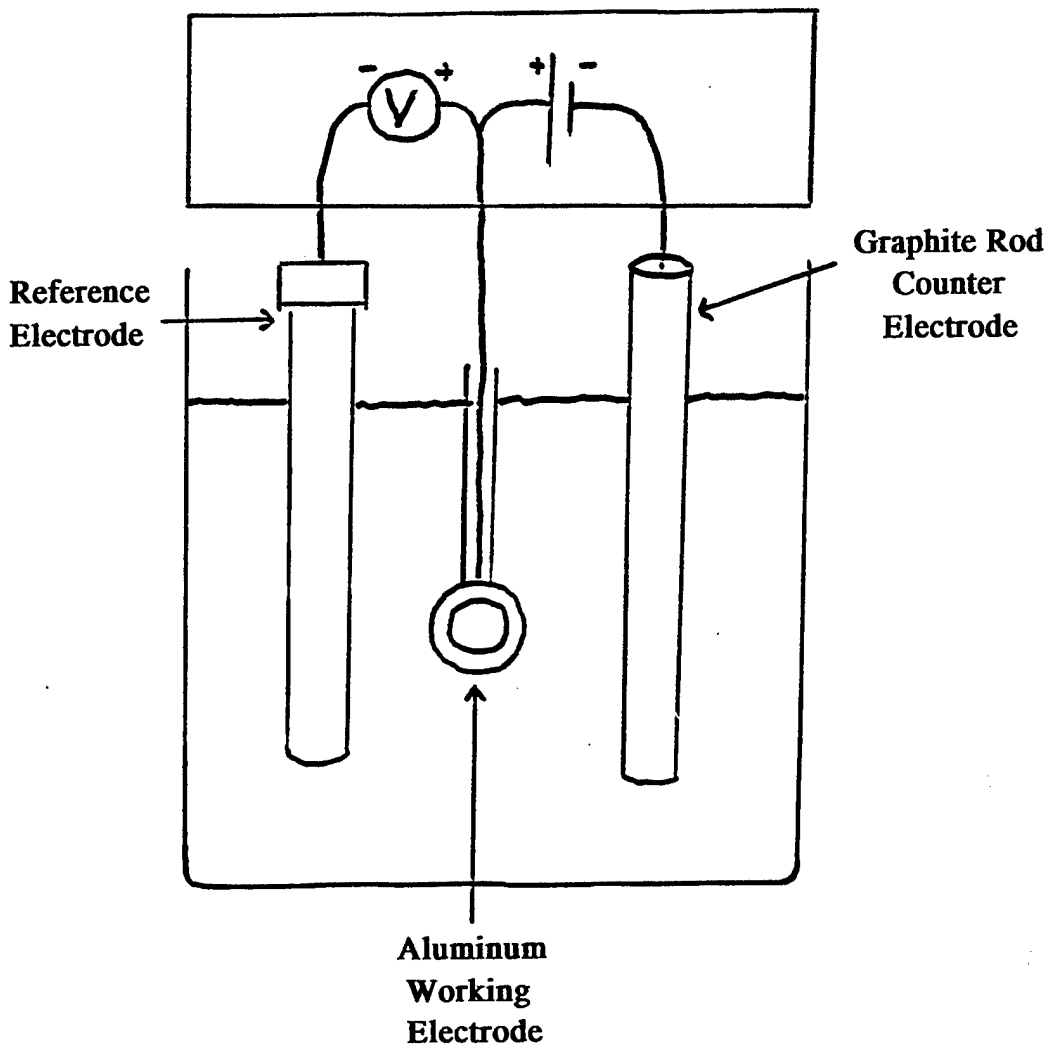

FIGURE 7: Electrochemical Cell test setup for metastable experiments.

was an M352 Corrosion software package from EG&G Princeton Applied Research Company. The potentiostat used was an EG&G Princeton Applied Research Versastat Potentiostat.

In order to insure that the reference electrode used in the experiments was accurate, it was tested against a standardized reference cell setup. The reference cell setup consisted of two new saturated calomel reference electrodes exposed in a supersaturated solution of potassium chloride. A voltmeter was used to test the voltage difference between these two benchmark reference electrodes to determine their accuracy. The voltage difference between the two benchmark electrodes was always less than 1 mV. This value was well within the experimental error of the measurement. Once the two benchmark electrodes were standardized against each other, a third electrode was measured against the two. This third electrode was the electrode that was used in all of the experiments during the project. The voltage potential found between the experimental electrode and the two testing electrodes before the metastable tests was a negative 15 mV. This negative 15 mV difference meant that the experimental reference electrode was displaying potentials 15 mV below their actual value. The voltage difference between the test

electrode and benchmark electrodes before the Ecorr and HCl tests was a negative 25 mV. These potential differences were input into the computer software, which compensated for them in the results so that all potentials were reported as a voltage relative to the true SCE potential +/- 1 mV.

METASTABLE TESTING

Metastable pitting examinations of polycrystalline aluminum as well as the three different single crystal orientations were conducted in the following manner. This test, as well as the other tests, were conducted at ambient temperatures, which ranged between 65 and 75 degrees Fahrenheit. The crystals were first prepared and mounted according to the above procedure and then inserted into the test solution. In order to simulate the seawater environment, a 3.5 % by weight sodium chloride in distilled water solution was prepared and inserted into the electrochemical cell. The electrochemical cell had a volume of 700 ml. This solution was prepared in bulk by adding 70 grams of sodium chloride to 2000 ml of distilled water. The solution was deaerated in the cell by vigorous nitrogen bubbling for 15 minutes. The deaeration was performed so

that the test solution would have low oxygen concentration (approximately 1ppm). A tube was connected from the exit of the bubbler to a beaker of water to ensure that there was a positive pressure in the cell from the nitrogen bubbling. Once the solution had been vigorously deaerated for 15 minutes, the potentiostatic tests were begun. While the tests were being conducted, the cell continued to be vigorously deaerated.

The metastable experiments were conducted by potentiostatically maintaining the potential at a certain value and monitoring the current density versus time using the computer software. Each potential was maintained for 10 minutes. After the 10 minutes, the potential was raised by 10 mV and the current density was again monitored. This procedure began at -785 mV vs SCE and continued in 10 mV steps until the last potential of -705 mV vs SCE was measured. A total of 5 experiments, each measuring from -785 mV to -705 mV vs SCE, were conducted on the polycrystalline aluminum as well as on each of the three single crystal orientations.

The data that were obtained from the metastable tests were in the form of current density versus time

measurements. An examination of these graphs allowed two separate assessments of the data. The first assessment examined the number of pitting events per surface area at each potential for each crystal orientation. Additionally, this assessment led to the determination of an experimental pitting potential for each crystal tested. At potentials below the pitting potential, there were relatively few pitting events. Once the potential reached and exceeded the pitting potential, the number of pitting events drastically increased, so much that the individual current spikes could not be discerned from the average current density. The pitting potential for the crystal was reached when the average current density masked the current spikes as mentioned above. This fact allowed the pitting potential of the individual orientations to be determined. The second assessment of the data was to record the peak pit current density at each potential for each crystal orientation. The peak pit current was defined as the largest current spike that occurred during the test.

Once the testing of each single crystal was complete, the crystal was removed from the cell and thoroughly rinsed with distilled water so that there was no test solution

remaining on the crystal. The crystal was then removed from the scrap piece of metal by cutting through the glyptal lacquer and pulling off the crystal. This was performed without touching or damaging the crystal face. Once removed, the single crystals were examined using a Hitachi S-800 Field Emission Scanning Electron Microscope located at the Naval Research Laboratory (NRL) for pit morphology as well as pit densities.

The scanning electron microscope examination was used to confirm that (100) faceted pitting had occurred on each crystal face. The microscope was used to focus on a single pit on the surface and examine the actual morphology of the inside of the pit. Using electron microscopy, the inside walls and their orientations were examined. Through an understanding of crystallography, the orientations of the facets within the pit were established.

A single crystal of each orientation was examined using a Jeol-6100 Scanning Electron Microscope located at the United States Naval Academy (USNA) in order to examine the number of pit sites for each orientation. Once placed in the microscope, the magnification was set to 300 times and each visible pit was counted for one quarter of the crystal

face. The quarter of the surface that was examined was chosen randomly. These pitting densities were compared for the three different orientations.

CORROSION POTENTIAL TESTING

The second series of tests involved testing the Ecorr of the different crystal orientations as a function of time. These experiments were conducted in the 3.5% by weight sodium chloride in distilled water solution. A single crystal of each crystal orientation was prepared according to the preparation procedure. All three single crystals were then placed in the test solution with a reference electrode and a nitrogen bubbler. The corrosion potential of each of the crystals was initially measured with a multimeter and the reference electrode located in the cell. The multimeter used for this experiment was a Fluke 77 Multimeter. In order to standardize the measurements, the corrosion potential was measured and recorded after the multimeter had been attached to the single crystal for 10 seconds. Once this first potential was measured, the solution was vigorously deaerated using nitrogen bubbling. This nitrogen bubbling continued for the duration of the

experiment to minimize the influence of the oxygen on the Ecorr of the single crystals. The corrosion potential of each of the crystals was measured and plotted versus the time in the solution. All three crystal orientations were evaluated during this test.

After 48 hours of corrosion potential measurements, the crystals were removed from the solution. They were then rinsed using distilled water and removed from the scrap metal holder. Each one of the crystals was examined using the scanning electron microscope at NRL for evidence of metastable or stable pitting.

A second corrosion potential test was conducted in the same manner as the first test. When the testing started, it was noticed that the Ecorr values of the (110) single crystal were immediately around the pitting potential and unstable. Because of this, the (110) crystal was removed from the solution and another (110) crystal was tested. The second (110) single crystal showed approximately the same Ecorr levels; however, they were more stable. This crystal was also removed from the electrochemical cell and the test was started with only the (100) and (111) single crystals. It was suspected that there was some problem in the mounting

of the (110) crystals, but this was not confirmed. After 3 hours of potential versus time measurements, each of the crystals, the (100) and the (111), was subjected to a potentiodynamic scan. Potentiodynamic scans were run at this time because the potential of the (111) crystal was beginning to increase and it was desirable to obtain the scan before the potentials neared the pitting potential. The crystals remained in the test solution and the nitrogen bubbling continued during the potentiodynamic scans. The scans began at a potential 200 mV above the latest corrosion potential measurement and were run until the potential was 300 mV below the latest corrosion potential measurement. The scanning rate for the test was 2 mV per second. The crystals remained in the sodium chloride solution after the scans and the Ecorr measurements continued. After 8 hours, another potentiodynamic scan was conducted on the (100) crystal to see if the reaction kinetics remained constant during the Ecorr experiment. By this time the (111) crystal had reached the pitting potential. After the potentiodynamic scan was taken on the (100) crystal, the test was ended and the crystals were removed from the solution and thoroughly rinsed with distilled water.

A third Ecorr test was conducted in the same manner as the first two with the exception of using a Keithley Multimeter. This multimeter was used because of the fact that it had a higher input impedance than the Fluke 77 Multimeter. However, the Ecorr measurements were ended after 8 hours so that potentiodynamic scans could be obtained on the crystals. The (111) crystal was removed from the test solution so that a graphite counter electrode could be inserted into the electrochemical cell. Once the graphite counter electrode was inserted in the test solution, potentiodynamic scans were taken on the remaining (100) and (110) crystals. Two sets of polarization curves were obtained. The first set obtained was a polarization curve from the corrosion potential to a potential 300 mV below the corrosion potential. The second set of polarization curves raised the potential from -880 mV to -700 mV vs SCE in order to monitor the pitting potential of the crystals. Once these curves were obtained, the crystals were removed from the solution and rinsed with distilled water.

HYDROCHLORIC ACID TESTING

A solution of hydrochloric acid was prepared at a pH of 4 by diluting 37.6 % hydrochloric acid with distilled water. The hydrochloric acid was purchased from J.T. Baker Chemical Company. The purity if the acid was ACS reagent purity. The hydrochloric acid was used as a test solution in order to simulate the pit chemistry. The pH was confirmed to be 4 by using pH paper.

The single crystals were prepared by the sample preparation method mentioned above. Additionally, the area of the crystals were determined so that results would be area normalized. The area was accurately determined by Dr. Paul Natishan at NRL with the use of a planimeter. The planimeter traced the outside of a magnified picture of the crystal. Once the entire perimeter of the exposed crystal face was traced, the planimeter displayed a certain number of units. In order to transfer these units to an area, the units were multiplied by a constant and the inverse of the magnification of the picture squared. Three measurements were conducted by the planimeter and averaged together in order to obtain an accurate value for each area.

The test setup included a beaker filled with the

hydrochloric acid test solution in which the saturated calomel reference electrode and a graphite counter electrode were located. The single crystals were tested in the hydrochloric acid individually. The crystals were placed in the solution at a conditioned potential so that they would not enter the solution at their Ecorr which would result in corrosion in the acidic solution. To accomplish this, a second graphite rod was inserted into the solution and potentiostatically held at -2.2 V vs SCE. Aluminum will not corrode at this potential in the acidic solution. The single crystals were placed electrically in parallel with the graphite rod, but outside of the solution. A conditioning time of 3 minutes was selected for the test. During this conditioning time the potential remained at -2.2 V vs SCE. Once the conditioning time of 3 minutes began, the single crystal was placed in the solution and then the graphite rod was removed from the solution. As soon as the 3 minute conditioning time ended, a potentiodynamic scan began from -2.2 V vs SCE to -2.8 V vs SCE at a rate of .75 mV per second. These potential values were selected so that the cathodic reaction could be evaluated. Once the potentiodynamic scan reached the final potential at -2.8 V

vs SCE, the potential was held at a conditioning potential of -2.2 V vs SCE for 3 minutes. During this time, the single crystal surface was polished with a clean Mastertex polishing cloth while it remained immersed in the hydrochloric acid solution. This polishing was performed by placing the polishing cloth on the tip of the investigator's finger and lightly polishing the surface of the crystal for 15 seconds. This polishing did not show any visible scratching of the crystal face. As soon as the polishing of the crystal was completed and the conditioning time ended, another potentiodynamic scan of the same potentials and scan rate as the first was conducted.

The polishing of the crystal at the conditioning potential was conducted so that the oxide layer on the crystal face could be removed or at least partially removed. While the entire oxide layer could not be removed from the crystal face because of the crude polishing technique, a significant portion of the passive barrier was likely removed. This polishing technique was performed on various crystals outside of the testing solution and the surfaces were examined with electron microscopy. The microscopy showed that the polishing resulted in an obvious removal of

some of the oxide barrier with minimal scratching of the crystal face.

Additionally, a (111) oriented crystal was prepared and inserted into the test setup as described above. The oxide layer was not removed from this crystal once it was in the solution. The crystal was subjected to 40 consecutive potentiodynamic scans from -2.2 V vs SCE to -2.8 V vs SCE with a 3 minute conditioning time between each scan. This experiment was performed to examine the cathodic kinetics as a function of time in the acidic solution. The data generated consisted of 40 separate curves on a single scale, which showed how the kinetics varied over the period of time.

Once the 40 potentiodynamic scans were completed, the (111) crystal was subjected to a potentiodynamic scan from -1000 mV vs SCE to -200 mV vs SCE at a rate of .5 mV per second. This scan monitored both the cathodic and anodic kinetics of the crystal in the acidic environment.

RESULTS AND DISCUSSION

METASTABLE TESTS

Metastable pitting experiments were conducted to examine the influence of crystal orientation on the initiation of pitting on aluminum. The protective oxide layer was removed from the crystals during the polishing. However, immediately after the crystals were removed from the polishing cloth, this oxide layer reformed in air due to its strong affinity to be oxidized. This oxide layer was present during the metastable test. The initiation phase of pitting involves the breakdown of this protective oxide layer and the subsequent anodic attack (dissolution) of the underlying aluminum. Because of the lack of any previous attack on the oxide layer prior to the testing, the metastable tests examined the initiation of pitting.

The first assessment of the metastable pitting tests provided data about the number of pitting events per area for 10 minutes as a function of crystal orientation. Sample data generated from a potentiodynamic scan at -745 mV vs SCE of a (110) single crystal are shown in Figure 8.

The definition of a pitting event for this data is any

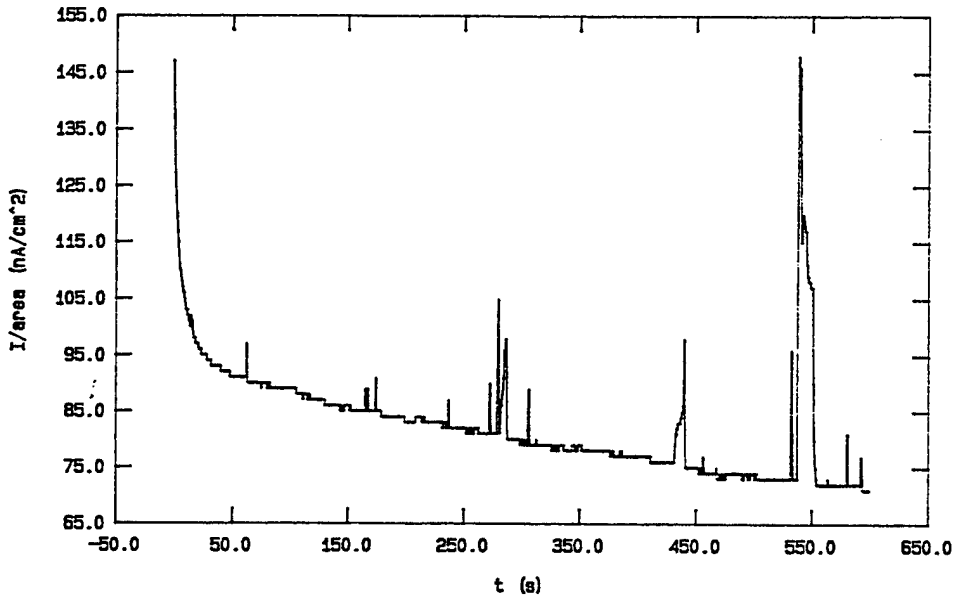

FIGURE 8: Potentiostatic measurement of current density vs time for a (110) single crystal at -745 mV vs SCE. This curve is a sample of the data that was generated during the metastable experiments.

current spike that exceeds the baseline average by more than 10%. This definition was utilized as a standard in order to qualify pitting events. The baseline for each current density versus time curve was established as the average current density value during the test. Each current spike was measured above this average value. Only the current spikes that exceeded the baseline by 10% were counted as metastable pitting events.

A graph showing the pitting events per area for polycrystalline aluminum and for each single crystal orientation is shown in Figure 9. These results showed that the crystals maintained similar metastable pitting characteristics until the potential reached -755 mV vs SCE. Above this value there evolved a dependence on the orientation for the number of pitting events. This showed that as the potential increased, the orientation of the crystal began to affect the metastable pitting. At -755 mV vs SCE, the (111) oriented single crystal began to show a significant increase in the number of metastable pitting events. The polycrystalline aluminum samples that were tested showed a similar large increase in the number of metastable pitting events at -755 mV vs SCE. As the

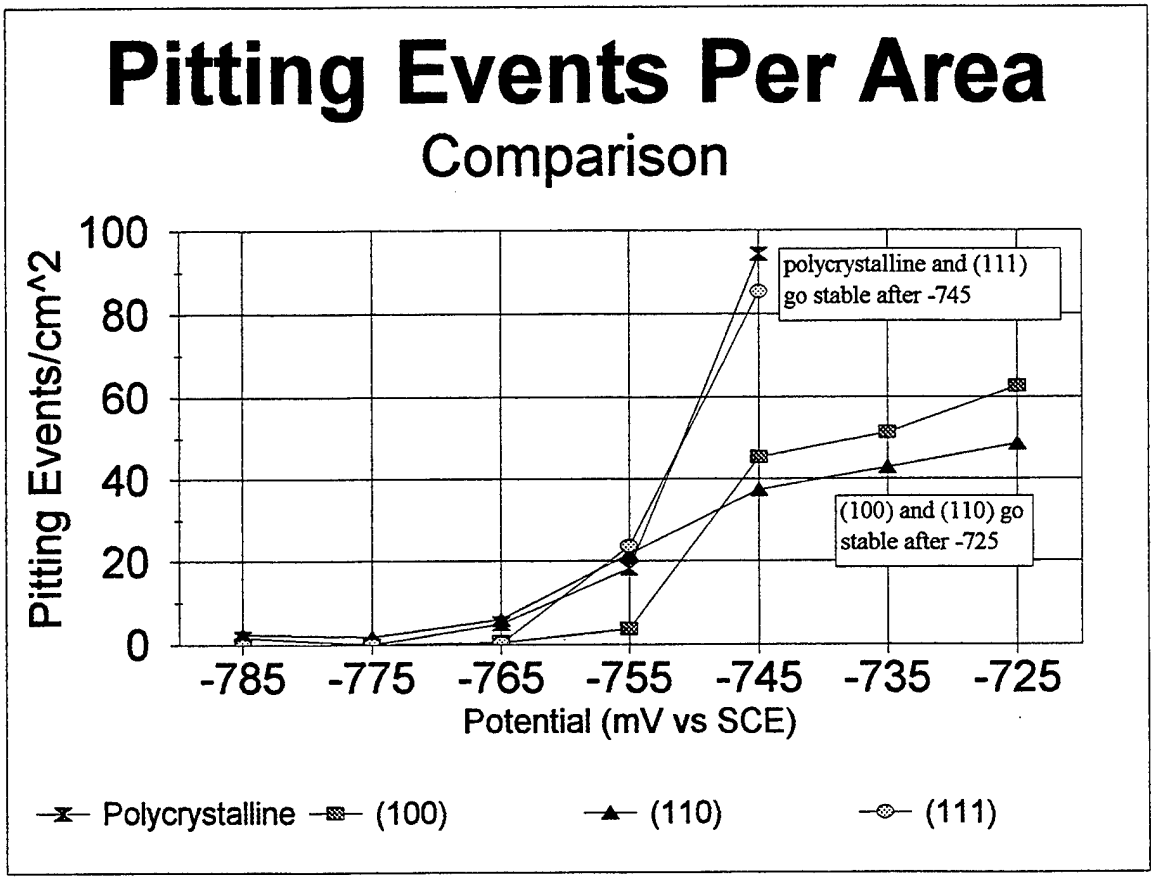

FIGURE 9: Relationship between the pitting events per area and the applied potential for (100), (110), and (111) single crystals and polycrystalline aluminum. The results were the average of 5 separate experiments for each aluminum crystal.

potential was increased for the other two single crystal orientations, (100) and (110), they experienced an increase in metastable pitting, yet not as much as the (111) orientation.

As the potential was increased, each of the aluminum crystals began to experience an increase in the number of current spikes. Figure 10 shows the increase in current spikes as the potential is increased. As the potential continued to be increased, the current spikes began to dominate the curves. This made it difficult to distinguish between a metastable pitting event and a stable pitting event. Because the current spikes gradually dominated the curve, there was a gradual transition from metastable pitting to stable pitting. This made it difficult to discern a precise pitting potential. The pitting potential was experimentally determined to be the point where the increase in the number of current spike made it impossible to count metastable events and when the current density showed a gradual overall increase during the 10 minute period. An increase in current density is caused by pits becoming stable and propagating.

The (111) single crystal experienced stable pitting at

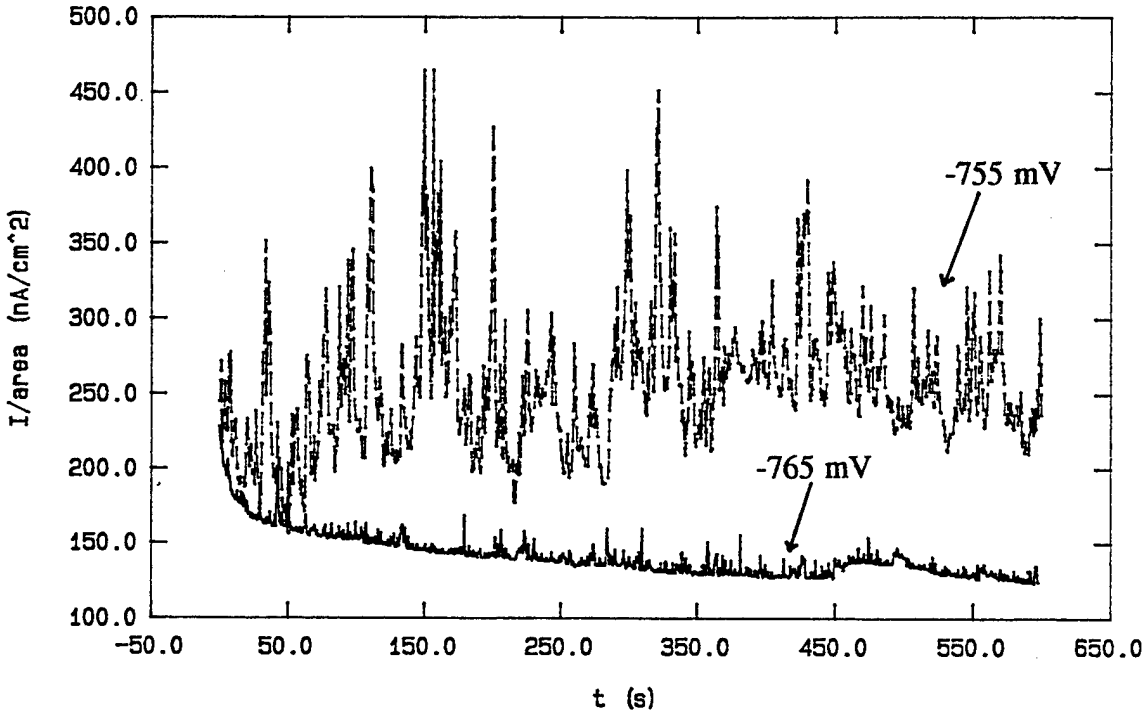

FIGURE 10: Results of two potentiostatic tests on a (111) single crystal at -765mV and -755mV vs SCE. These results showed how the frequency and height of the current spikes increased with increasing potentials.

potentials above -745 mV vs SCE. This stable pitting meant that the (111) single crystal had reached its pitting potential. Experimentally the pitting potential was established between -745 mV and -735 mV vs SCE. The polycrystalline crystals also experienced stable pitting between -745 mV and -735 mV vs SCE. Both the (100) and (110) single crystals showed a transition to what appeared to be stable pitting between potentials of -725 mV and -715 mV vs SCE. It is important to note that the standard deviations associated with each orientation did not overlap at the higher potentials, where the most significant differences in the average values occurred.

Yasuda et al. found the pitting potential of the (111) orientation to be -739 mV vs SCE [8]. They also found that the pitting potentials for the other two crystal orientations were -724 mV vs SCE for the (110) orientation and -700 mV vs SCE for the (100) orientation. In general, the findings described above were in close agreement with the results of Yasuda et al in that the pitting potential of the (111) crystal was greater than the pitting potential of the other two oriented crystals.

The results of the present work showed that the (111)

single crystal had more pitting events per area than the other single crystal orientations. This indicated that this orientation was the most susceptible to metastable pitting. It was also observed that this orientation was more susceptible to initiation of stable pitting. Also, because stable pitting occurred at a lower potential for the (111) orientation than for the other orientations, it appears that the stable pit chemistry is more readily maintained at lower potentials for the (111) orientation. Additionally, the resemblance of the polycrystalline metastable pitting results and the (111) metastable pitting results indicated that the (111) orientation strongly affects the metastable pitting as well as the pitting potential of polycrystalline aluminum. Another possible explanation for the large amount of metastable pitting on the polycrystalline aluminum could be that the grain boundaries on the surface contributed to metastable pitting.

The peak pit currents during the metastable tests were recorded in order to determine if they were a function of crystal orientation. A larger peak pit current indicates that the pit corroded faster initially during a metastable pitting event. The peak pit current was defined as the

highest current value that occurred during a pitting event. A diagram showing a peak pit current is shown in Figure 11. Since the current was directly proportional to the initial rate of aluminum dissolution, higher peak pit currents should correspond to larger metastable pitting events, i.e. more corrosion, assuming the duration of the pitting events were approximately the same. The results of the tests are shown in Figure 12. The data showed that as the potential was increased, the value of the peak pit current increased. This occurred because the higher the potential, the faster the dissolution rate and the more easily the pit chemistry was maintained. The data showed that the orientation of the single crystal had no effect on the peak pit current below the pitting potential; -745 mV vs SCE for the (111) orientation and between -715 mV and -725 mV vs SCE for the other two orientations. Once the pitting potential for polycrystalline aluminum was exceeded, the results showed that the average peak pit currents exhibited a dependence on the crystal orientation. The average peak pit currents were largest for the (111) crystal and smallest for the (100) crystal. Below the pitting potential of polycrystalline aluminum, the behavior of the three orientations varied and

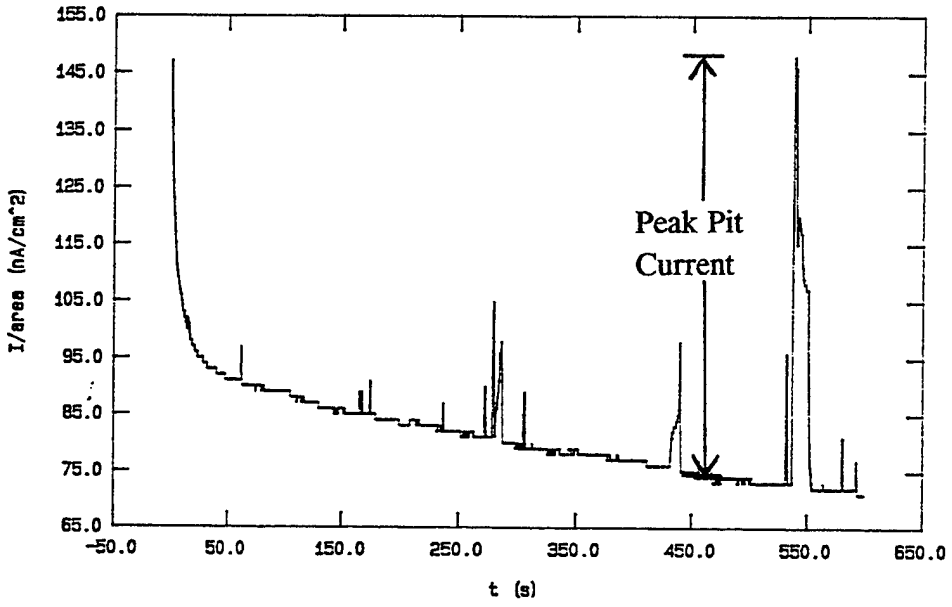

FIGURE 11: A peak pit current is shown on a current density versus time graph. These graphs were generated during the metastable pitting experiments.

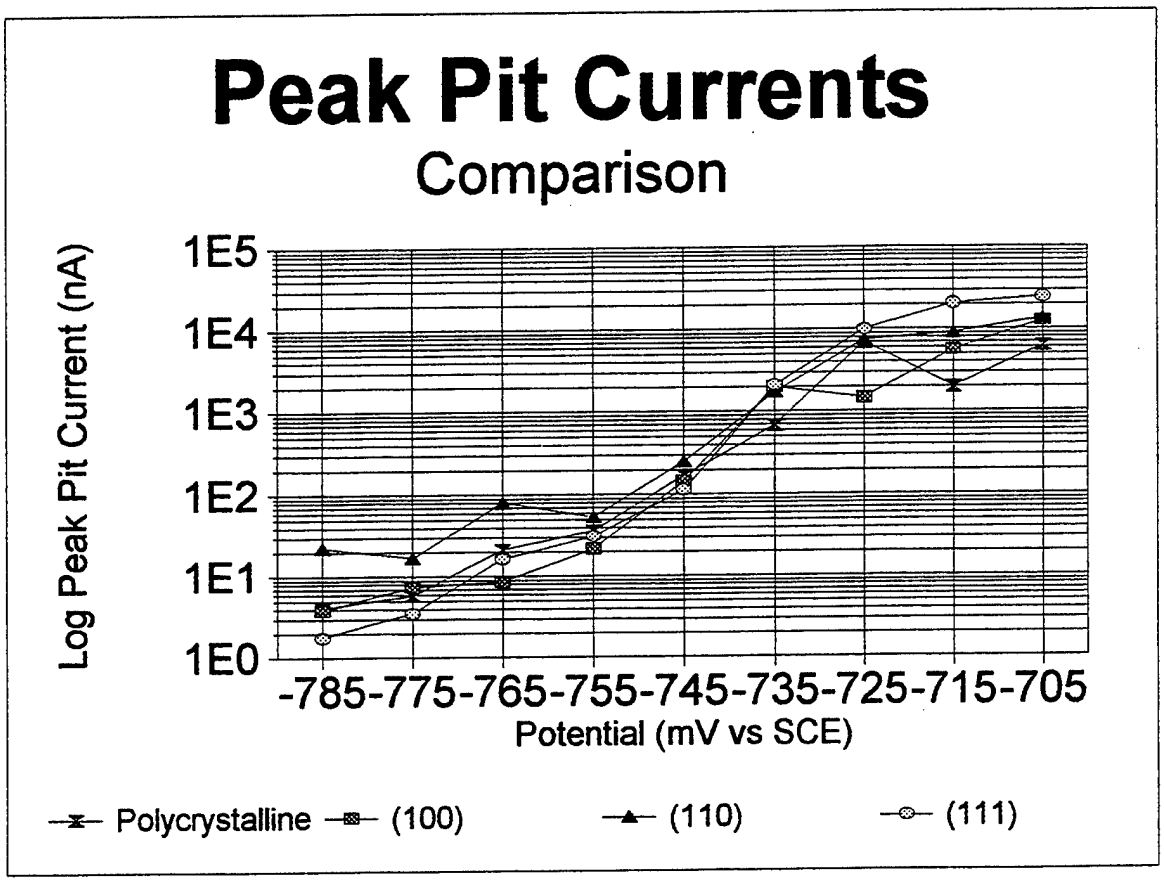

FIGURE 12: Relationship between the peak pit currents and the applied potential for (100), (110), and (111) single crystals and polycrystalline aluminum. The results were the average of 5 separate experiments for each aluminum crystal.

no clear trend was observed. However, the averages of the data contained large standard deviations that overlapped between the crystal orientations.

For the average peak pit current values only, the results matched the results found for the number of pitting events per area. This lends some more credibility to the concept that the (111) orientation corrodes faster and can best support the critical pit chemistry at the pitting potential of polycrystalline aluminum, while the (100) has the least ability to support the critical pit chemistry at this potential. This leads to the argument that the aluminum dissolution rate, $Al \rightarrow Al^{+3} + 3e^-$, must be in the following order: (111)>(110)>(100) at the pitting potential of polycrystalline aluminum.

Pitting density examinations were also conducted subsequent to the metastable tests and they showed the pitting of aluminum to be anisotropic. The results of the electron microscopy examination were that the (100) oriented single crystal had 435 micropits per square centimeter, the (110) single crystal had 675 micropits per square centimeter, and the (111) single crystal had 725 micropits per square centimeter. These results show that the pitting

density of the single crystals are in the increasing order: (100), (110), (111). This data also showed that the (111) single crystal had the highest affinity for pitting while the (100) single crystal had the least affinity for pitting. From these results, the corrosion resistance of the single crystals lie in the following increasing order: (111), (110), (100).

A single crystal of each orientation was examined after the metastable testing using the scanning electron microscope at NRL in order to determine the pit morphology of each orientation. The results of the microscopic examination showed that when each oriented crystal pitted, the resultant morphologies within the pit were (100). The (100) crystal exhibited rectangular pits, whose walls were orthogonal to the surface orientation (Figure 13). The (110) single crystal exhibited v-shaped pits with the (100) orientations as the walls of the pit (Figure 14). The (111) single crystal exhibited tetrahedral shaped pits pointing downward (Figure 15). These tetrahedral shaped pits consisted of three (100) orientations that met at a point, or corner, at the bottom of the pit. These pits were triangular shaped at the surface. These results confirmed

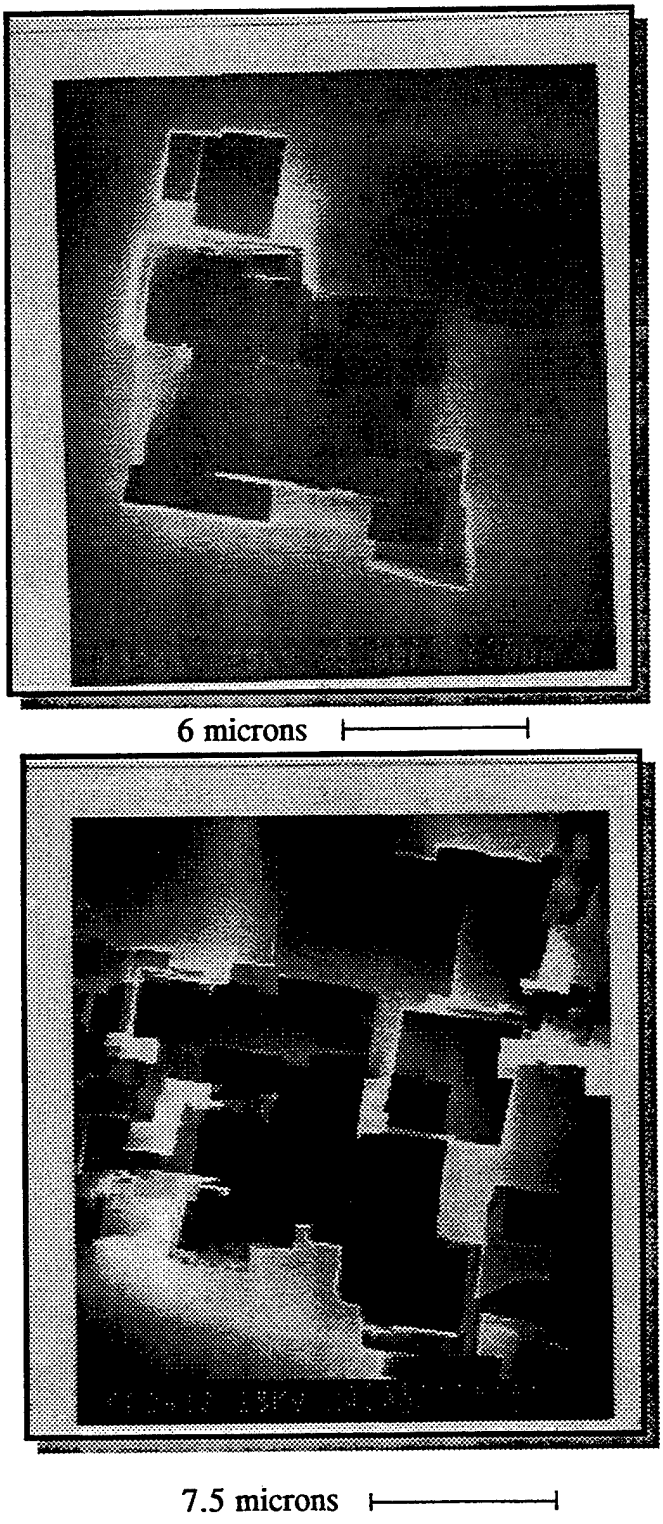

FIGURE 13: SEM micrographs of rectangular pitting morphology on a (100) oriented crystal.

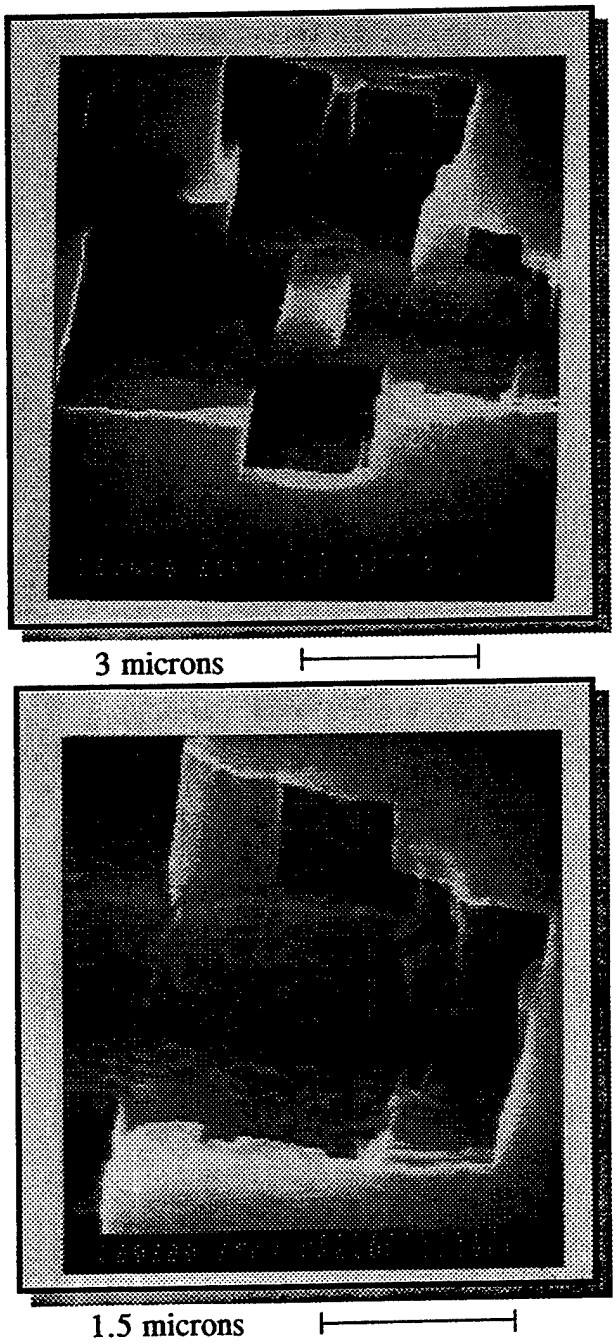

FIGURE 14: SEM micrographs of V-shaped pitting morphology on a (110) oriented crystal.

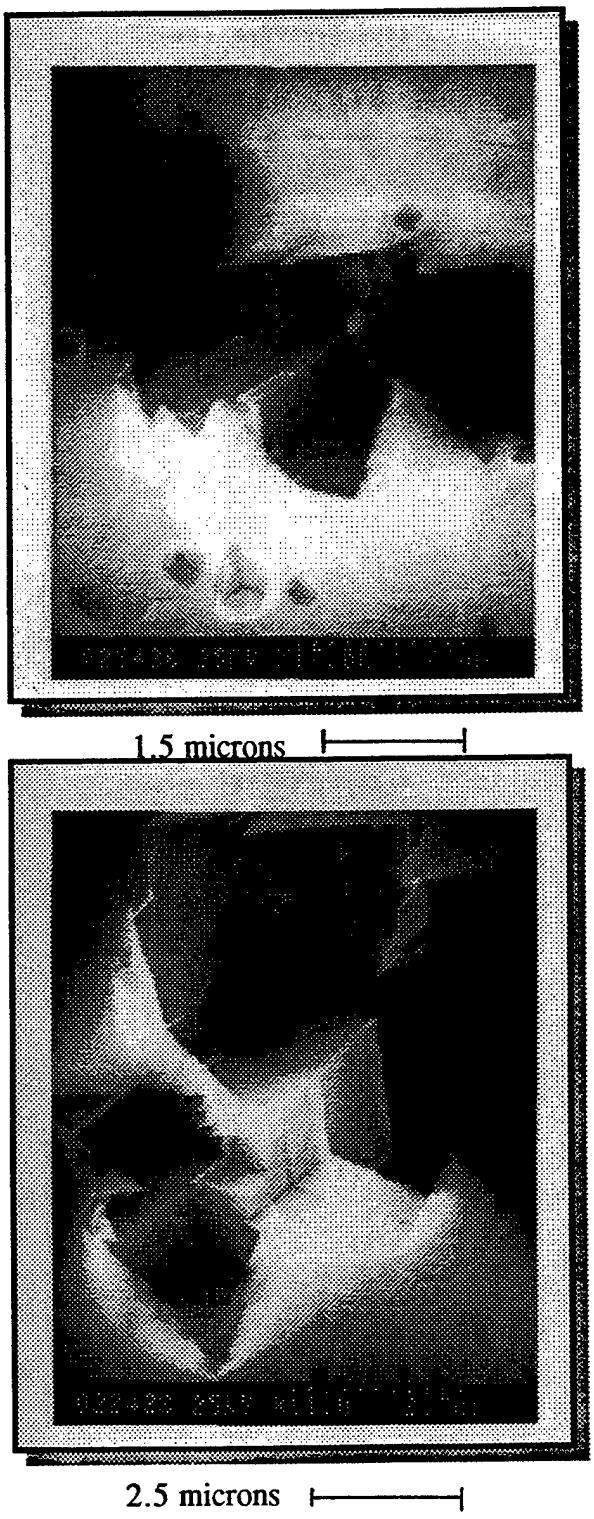

FIGURE 15: SEM micrographs of tetrahedral pitting morphology on a (111) oriented crystal.

that when the aluminum pitted, the resultant orientations of the exposed face within the pits were (100) orientations.

CORROSION POTENTIAL TESTS

The Ecorr experiments were conducted to examine the reaction kinetics of the aluminum single crystals. As previously mentioned, a material's Ecorr is the potential at which the metal exists in its environment. Because this potential occurs at the intersection of the anodic and cathodic curves, it is important to know where this potential is for a material. Any differences in the Ecorr value for the different orientations are due to a difference in the cathodic reaction rate and or the anodic reaction rate. This was why the Ecorr tests were conducted.

The results of the first Ecorr experiment, i.e. the Ecorr as a function of time for the three crystal orientations, are shown in Figure 16. From this data, it can be observed that the Ecorr values for all three potentials quickly dropped to below -1000 mV vs SCE. After 10 minutes, the Ecorr of the (111) single crystal began to rise. This rise continued for 5 hours until it neared the pitting potential and then the crystal began to show

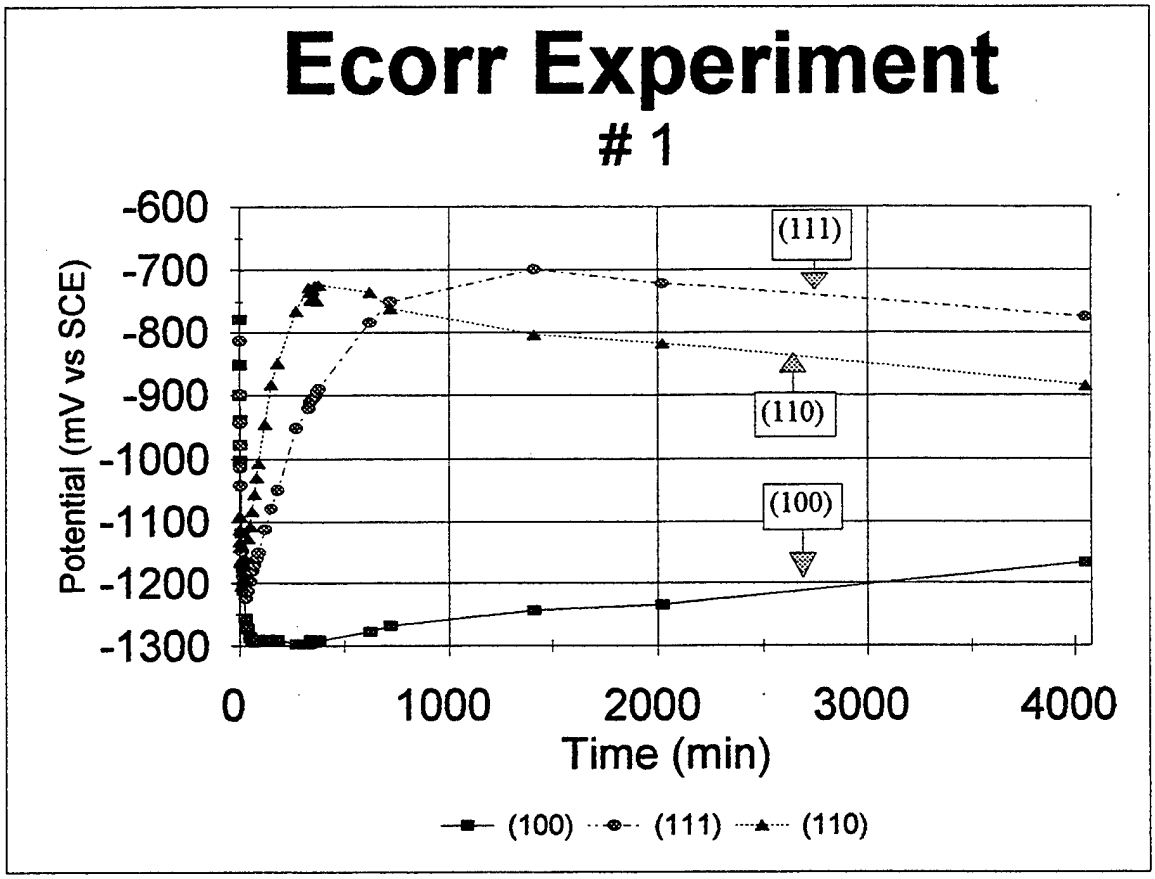

FIGURE 16: Relationship between the corrosion potential and time for a (100), (110), and (111) single crystal for the first Ecorr experiment.

instability in its Ecorr. During the 10 second measurements the Ecorr varied by as much as 100 mV within the 10 second measurement period. This range still centered around the pitting potential. After 7 hours of instability the Ecorr began to stabilize and eventually decreased as well. After 48 hours, the Ecorr had fallen to -884 mV vs SCE. The (110) showed similar behavior to the (111) crystal. The (110) crystal Ecorr took 30 minutes to begin to increase. The Ecorr reached the pitting potential and became unstable after 24 hours. After 5 hours of instability the Ecorr began to decrease. The Ecorr of the (100) crystal showed a great deal of stability and maintained a low potential. Initially, as the solution was deaerating, the crystal's Ecorr slowly decreased. Once the solution was essentially void of oxygen, the Ecorr maintained its value between -1200 mV vs SCE and -1300 mV vs SCE. This is typical behavior for aluminum and aluminum alloys in a deaerated sodium chloride solution.

From the electron microscopic examination of the three single crystals from the first Ecorr test, there was convincing evidence of pitting damage on the (111) single crystal, but not on the surface of the other two

orientations. This pitting damage was difficult to discern due to the presence of additional oxide growth on the surface of the crystals (Figure 17). It has been shown that these oxides form when aluminum remains in the solution for an extended period of time [11]. The possible oxide layer, in the present study, appeared to be pseudo-boehmite and bayerite forms of aluminum oxide by comparison to electron micrographs presented by Alwitt [11]. Evidence of these oxides were found on all three crystals, yet the oxides appeared to be thicker on the (111) single crystal. Also, the oxides on the (100) crystal appeared to have areas that had not completely covered the surface (Figure 18). The areas of the possible oxide that had not filled in could have been shallow pits. However, this is doubtful because there was no evidence of crystallographic attack and because the crystal was nowhere near the pitting potential during the experiment. Because of this oxide growth, pits could have been masked on the (100) as well as on the (110) single crystals. Nevertheless, there was visible pitting damage on the (111) crystal (Figure 19), indicating that the (111) crystal experienced metastable and possibly stable pitting.

A second Ecorr test was run to see if the data obtained

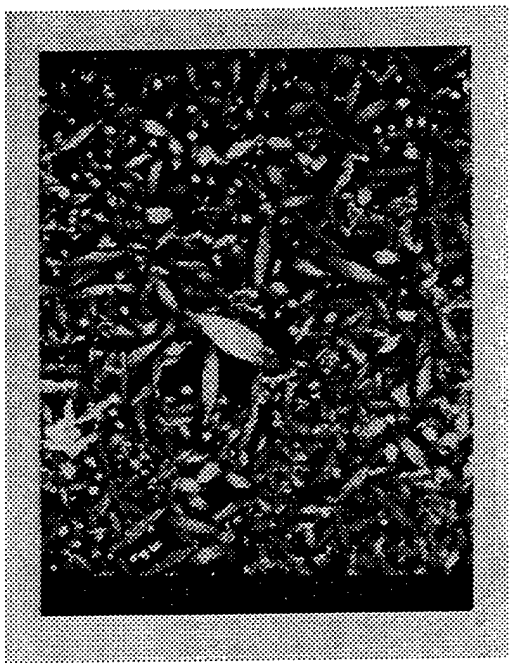

15 microns

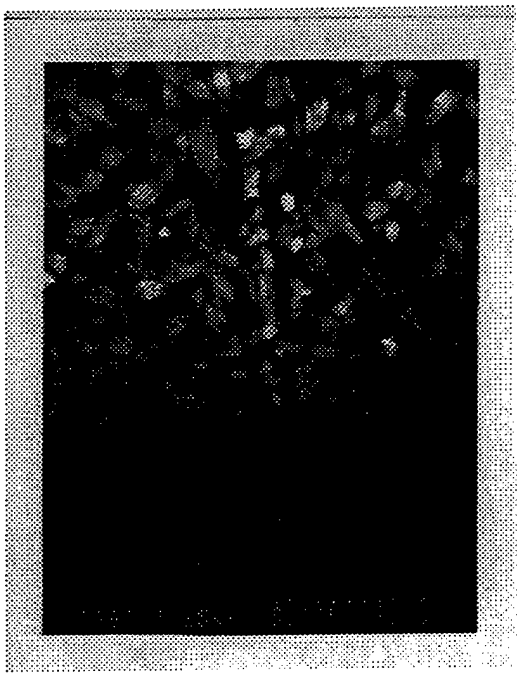

6 microns

FIGURE 17: SEM micrographs showing the oxide formation on the single crystals after the first Ecorr test. These oxides appeared to be pseudo-boehmite and bayerite forms of aluminum oxide.

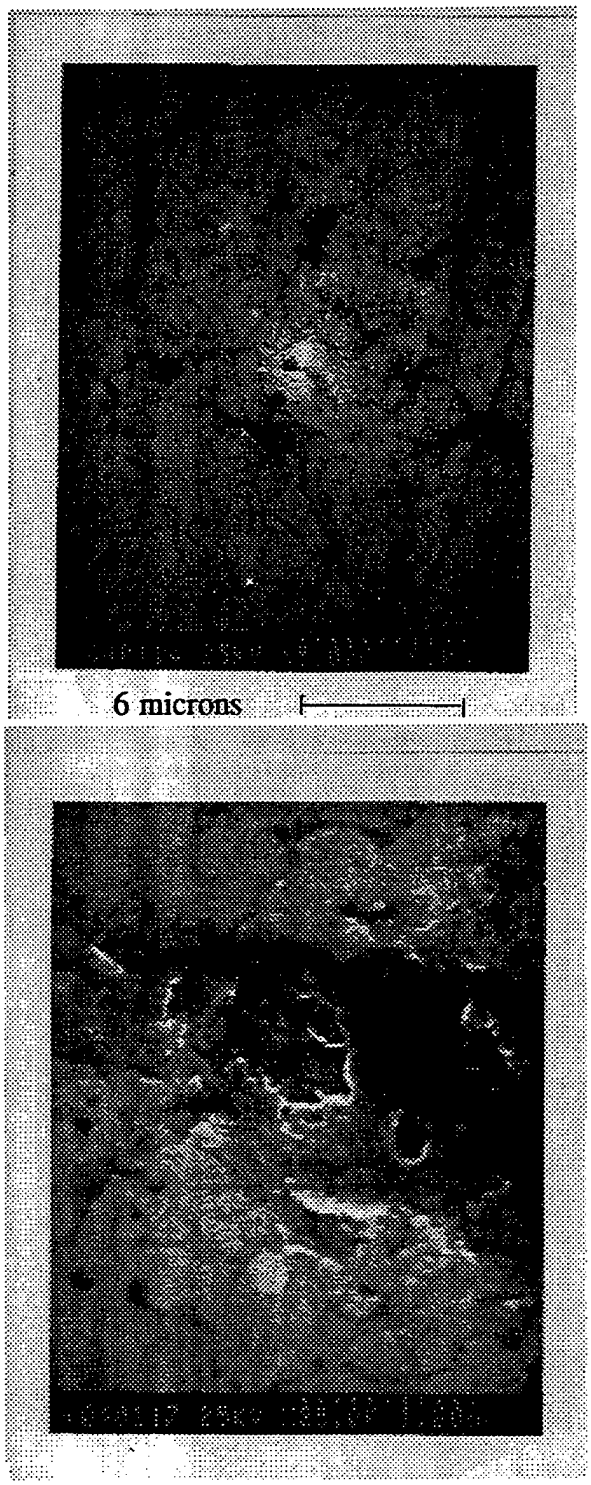

FIGURE 18: SEM micrographs showing the incomplete oxide formation on the (111) single crystal after the first Ecorr test.

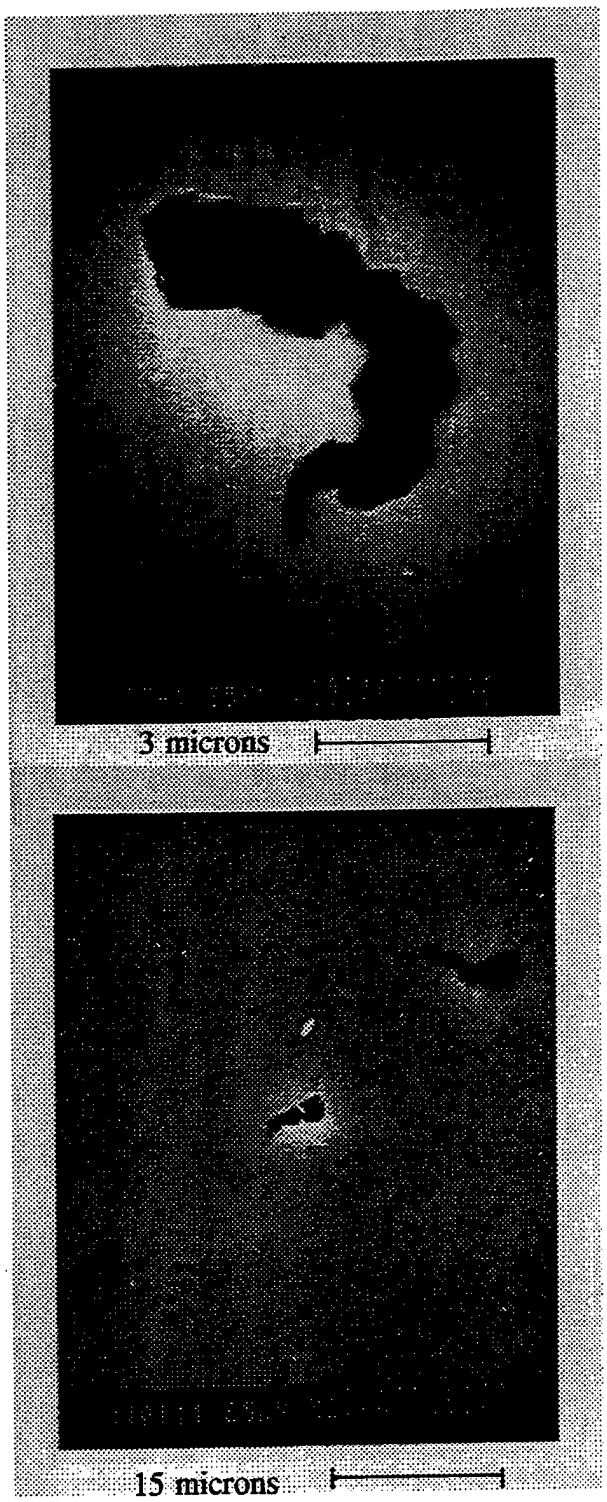

FIGURE 19: SEM micrographs showing the crystallographic pitting on the (111) crystal after the first Ecorr test.

in the first test was reproducible. The second test consisted of only a (100) single crystal and a (111) single crystal as described previously. The Ecorr vs time curve obtained during this test closely resembled the curve for the first test (Figure 20). The Ecorr measurements were stopped for both crystals once the (111) single crystal Ecorr began to increase near the pitting potential. Polarization curves were then conducted on each crystal as described earlier. From these curves (Figure 21), the difference between the cathodic reactions of the two single crystals can be seen. The cathodic kinetics were more active on the (111) crystal than the (100) crystal. This was deduced from the fact the cathodic reaction line was farther to the right (more active) on the polarization curve for the (111) crystal than for the (100) crystal. The second polarization curve on the (100) crystal, obtained after 8 hours, closely resembled the first curve (Figure 22). This showed that the reaction kinetics on the (100) crystal remained the same during the Ecorr experiment.

The first two tests used a Fluke 77 Multimeter to record the Ecorr values. This multimeter had an input impedance of 10^7 Ohms. It was found that the impedance of

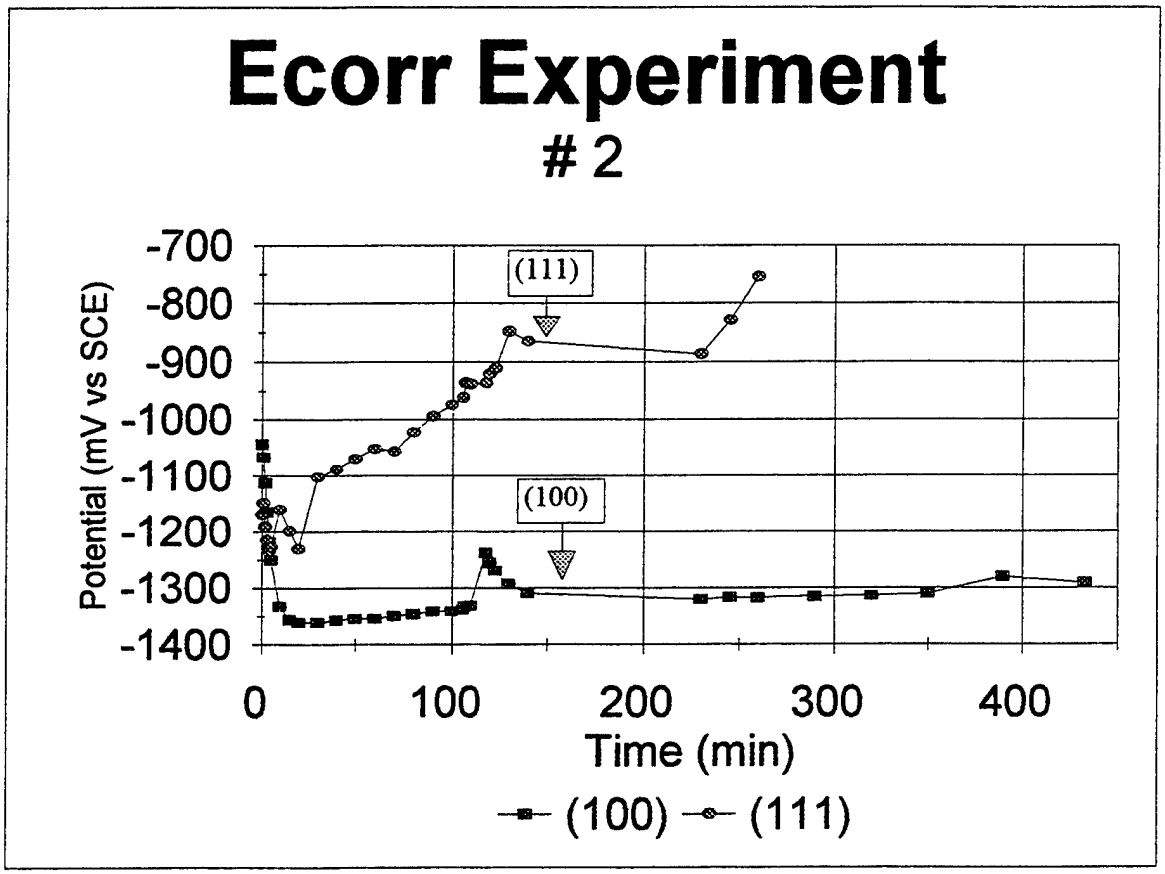

FIGURE 20: Relationship between the corrosion potential and time for a (100) and (111) single crystal for the second Ecorr experiment.

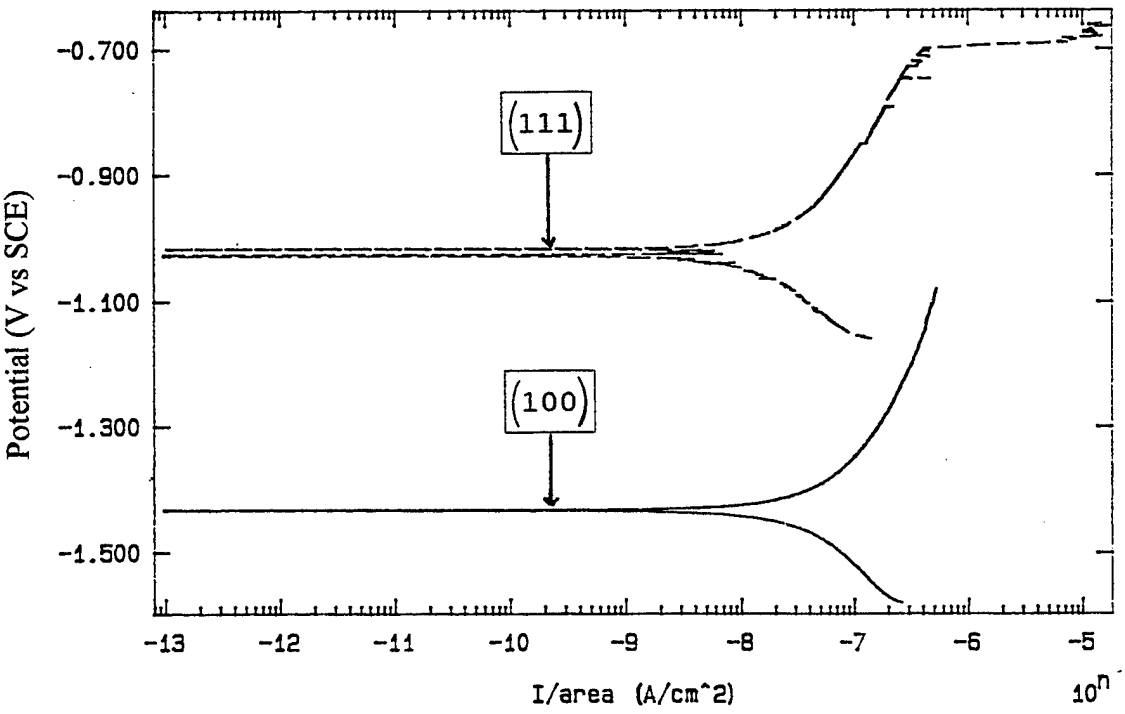

FIGURE 21: Polarization curves on the (100) and (111) single crystal used in the second Ecorr experiment. These curves show the large difference between the rates of the cathodic reactions.

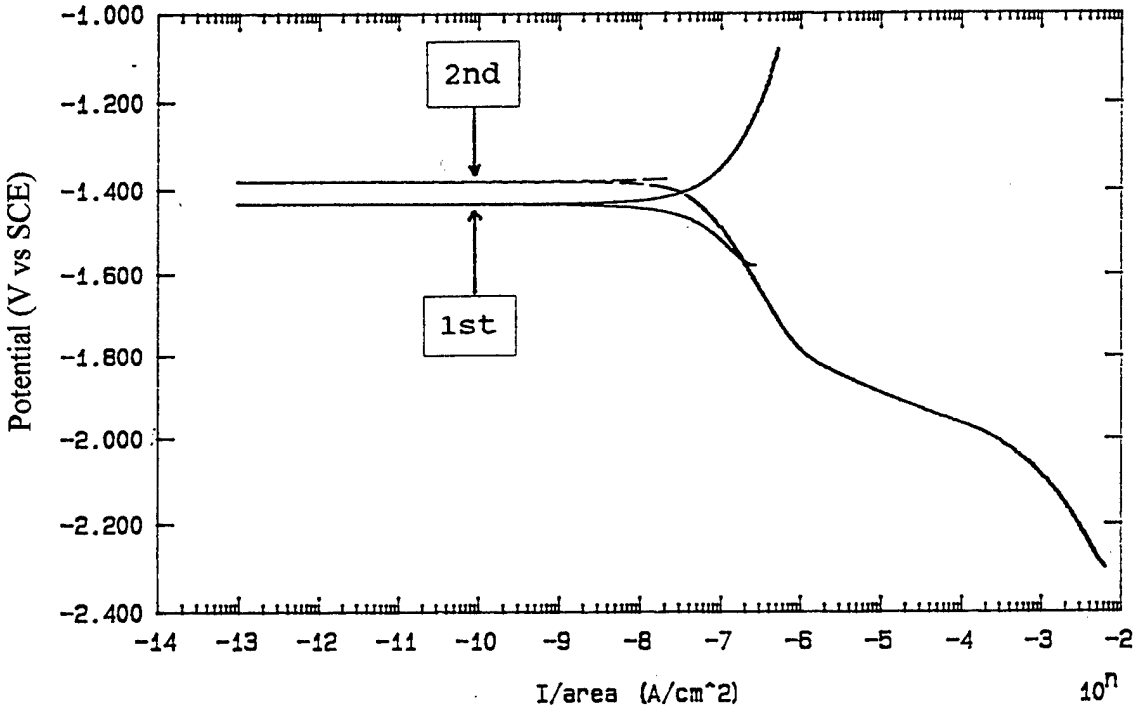

FIGURE 22: First and second polarization curves on the (100) single crystal used in the second Ecorr experiment. The similarity between the two curves showed that the reaction kinetics remained the same during the experiment.

the multimeter was not high enough to prevent the multimeter from polarizing the single crystals. The multimeter, when connected to the single crystals, raised the potential of the crystals by 100 to 150 mV. Although this polarization of the crystals by the multimeter raised the potential, it did not affect the general corrosion behavior of the aluminum crystals, i.e. the increase in potentials for the (111) crystal and the relatively constant low potential for the (100) crystal. In order to monitor the Ecorr without polarizing the crystals, a Keithley multimeter was used in the third test. This multimeter had an input impedance of 10^{12} Ohms. This input impedance was high enough to prevent the multimeter from polarizing the crystals.

The third Ecorr test was run for all three orientations for the purpose of removing the crystals after the Ecorr had reached the pitting potential and been unstable for approximately 3 hours. If the crystals had been taken out when they had been at the pitting potential for several hours then metastable pits should have been evident on the surface because the exposure time was such that the oxide would not thicken appreciably as had occurred in the first Ecorr test. As soon as the test began, it was evident that

this data was not reproducing the same curve as the previous two tests (Figure 23). The Ecorr was decreasing initially like the first two tests. However, the Ecorr remained at low potentials for the (110) and (111) crystals as opposed to starting to increase. The potential of the (100) crystal gradually increased as opposed to remaining at low potentials. The experiment was run for 7 hours and then polarization curves (Figure 24) were taken for the (100) and (110) single crystals to compare them to the polarization curves in the second test. A polarization curve was not taken for the (111) crystal because it was removed so that the graphite counter electrode could be inserted. The polarization curves for the two crystals were completed in two steps. The first step was to potentiodynamically scan the single crystals to potentials below the Ecorr to examine the cathodic reactions. The second step was to potentiodynamically scan the single crystals to potentials above the Ecorr to analyze the anodic reactions. These polarization curves showed that (100) crystal had a more active cathodic reaction line than the (111) crystal. This data contradicts the polarization curves produced during the second Ecorr test. The anodic scans of the two crystals

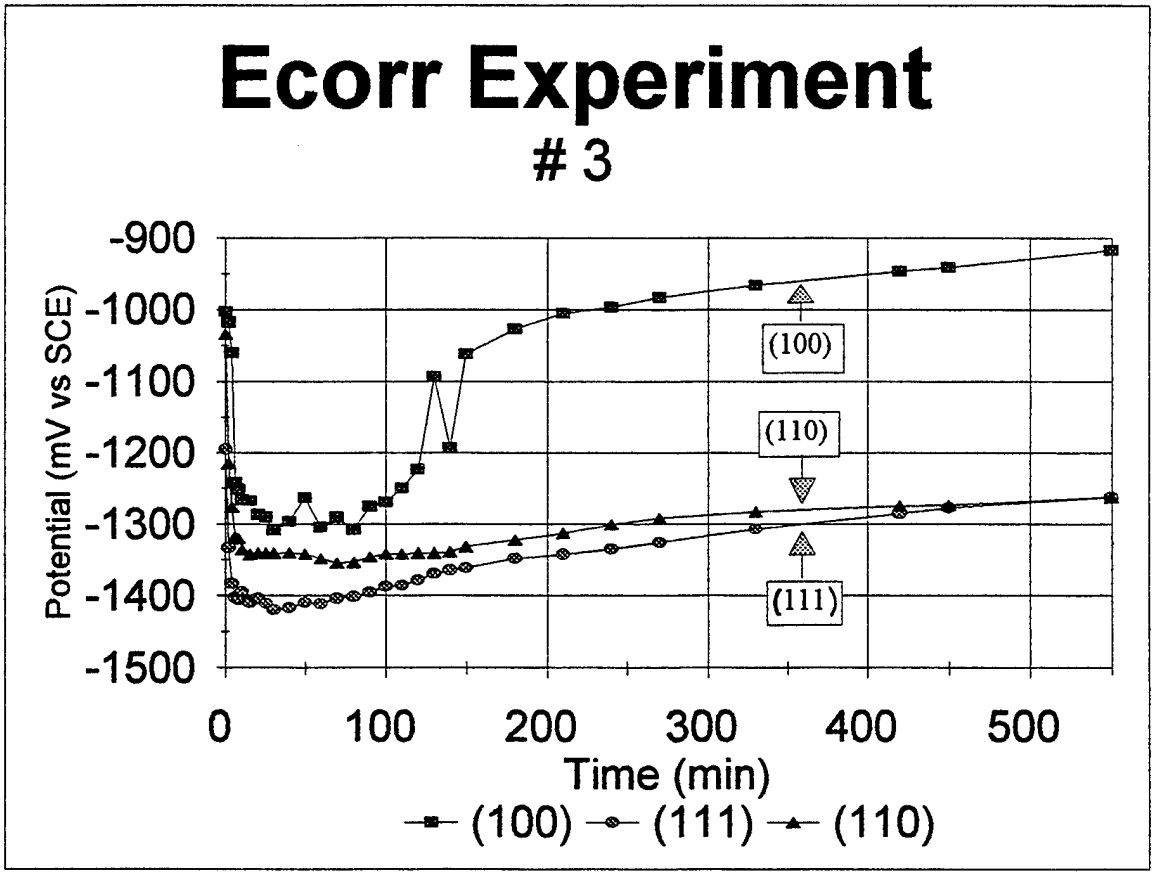

FIGURE 23: Relationship between the corrosion potential and time for a (100), (110), and (111) single crystal for the third Ecorr experiment.

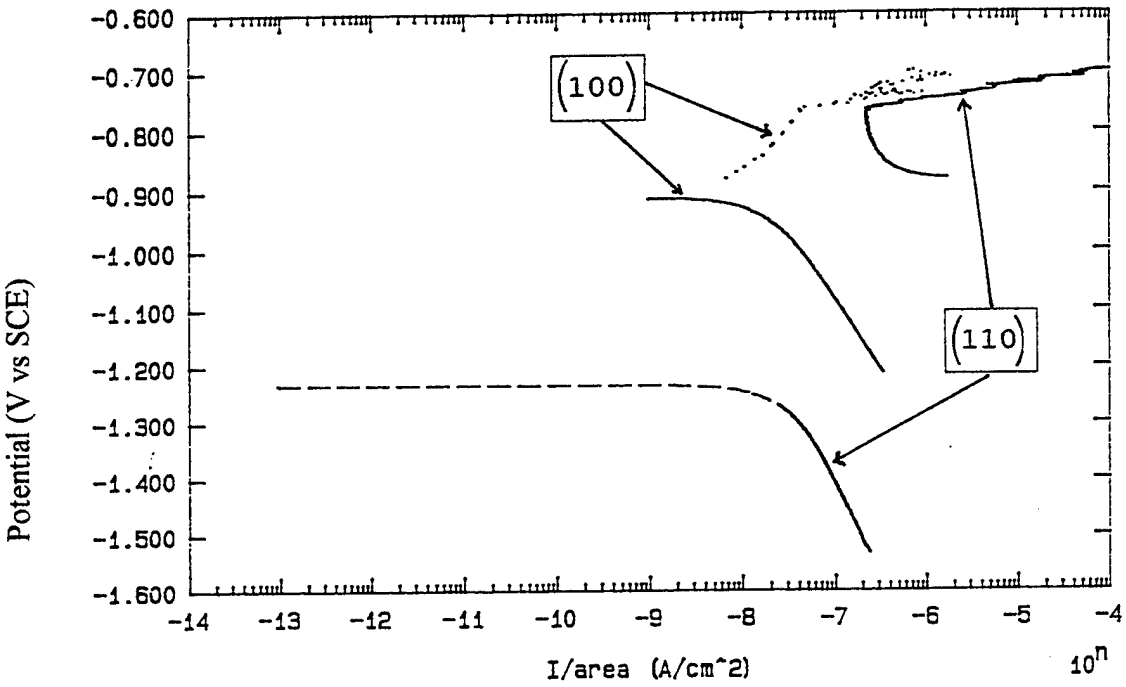

FIGURE 24: Polarization curves on the (100) and (110) single crystals used in the third Ecorr experiment. These curves showed both the anodic and cathodic reaction rates.

showed that the crystals experienced pitting in the region expected.

It is not known why the third Ecorr test did not reproduce the results found in the first two Ecorr tests. It is also not understood why the Ecorr of any of the single crystals began to rise to the pitting potential. One explanation for this rise could be the coexposure of carbon with the aluminum crystals. Carbon was experimentally determined to have a very high Ecorr value, +241 mV vs SCE, and this could have pulled the Ecorr of the aluminum crystals in a more positive direction if there was coexposure of the aluminum and graphite.

The coexposure of the carbon could have occurred due to one of two different factors. First, the glyptal may not have properly sealed the crystal and the carbon cement may have been exposed to the solution. This explanation is highly unlikely because of the care taken in ensuring that the crystal faces were isolated with the glyptal. It is also possible that the single crystals were contaminated with aluminum carbides. Since the single crystals were grown in a graphite mold, it is possible that some carbon entered into the metal solution as the crystals were being

grown. This explanation was not further explored because it required highly sophisticated instrumentation and resources beyond those available.

Additionally, it is not understood why the Ecorr began to fall for some of the crystals after it remained at the pitting potential for a period of time. There are two possible explanations that could explain this decrease in the Ecorr. First, it could be attributed to the formation of aluminum oxides on the surface. These oxides could have lowered the Ecorr value on the crystal surface [11]. It is also possible that the decrease in Ecorr was due to metastable pitting. It was found that the (100) crystal had the lowest Ecorr values of the three crystals in the first two Ecorr tests. If the (111) and (110) single crystals began to pit when they were near the pitting potential, then they would pit crystallographically, forming (100) orientations in the pits. These (100) orientations, which had lower Ecorr values in the first two tests, could have pulled the overall Ecorr value of the crystals in a more negative direction.

If the first two Ecorr tests were not flawed, then an important hypothesis can be made about the data. The

hypothesis is that the (111) single crystal is more cathodically active. This statement is based on the fact that the cathodic reaction line was much higher for the (111) crystal orientation than the (100) crystal orientation (Figure 24). A higher cathodic reaction line for the (111) crystal means that the cathodic current density is greater at a given potential on the surface of the (111) crystal than the (100) crystal. In order for the anodic dissolution of a metal to occur, there needs to be a cathodic reaction to balance the reaction. Slow cathodic kinetics will limit the anodic kinetics of the corrosion based on this necessary balance. Since, the cathodic kinetics may have been more active for the (111) orientation, this would support faster anodic dissolution of the aluminum.

HYDROCHLORIC ACID TESTS

Hydrochloric acid tests were conducted in order to evaluate the dependence of crystal orientation in a simulated pit chemistry. It has not been determined if an oxide layer is present on the surfaces in the inside of a pit. Therefore, the testing of the single crystals was performed with the oxide layer present and after a portion

of the oxide layer had been removed in the acidic solution.

During the potentiodynamic scans of the three crystal orientations, both with and without the entire oxide layer, hydrogen evolution was continually observed on the surface of the crystals. Based on this fact and the fact that the environment was acidic, the cathodic kinetics that were monitored were essentially entirely due to the hydrogen reaction. It is important to point out that only a portion of the potentiodynamic scans can be used for an accurate comparison. During all of the scans, the hydrogen bubbles collected on the surface as the hydrogen evolution proceeded. Once these bubbles collected to an appreciable extent, they began to mask the cathodic kinetics on a portion of the surface of the crystal because they effectively reduced the area that was exposed to the solution. This masking can be seen on the potentiodynamic curves where the curve bends downward at the lowest potentials.

The crystals with a portion of the oxide removed showed greater cathodic current densities than the crystals without the oxide removed for each orientation (Figures 25-27). This result showed that the bare aluminum was more active

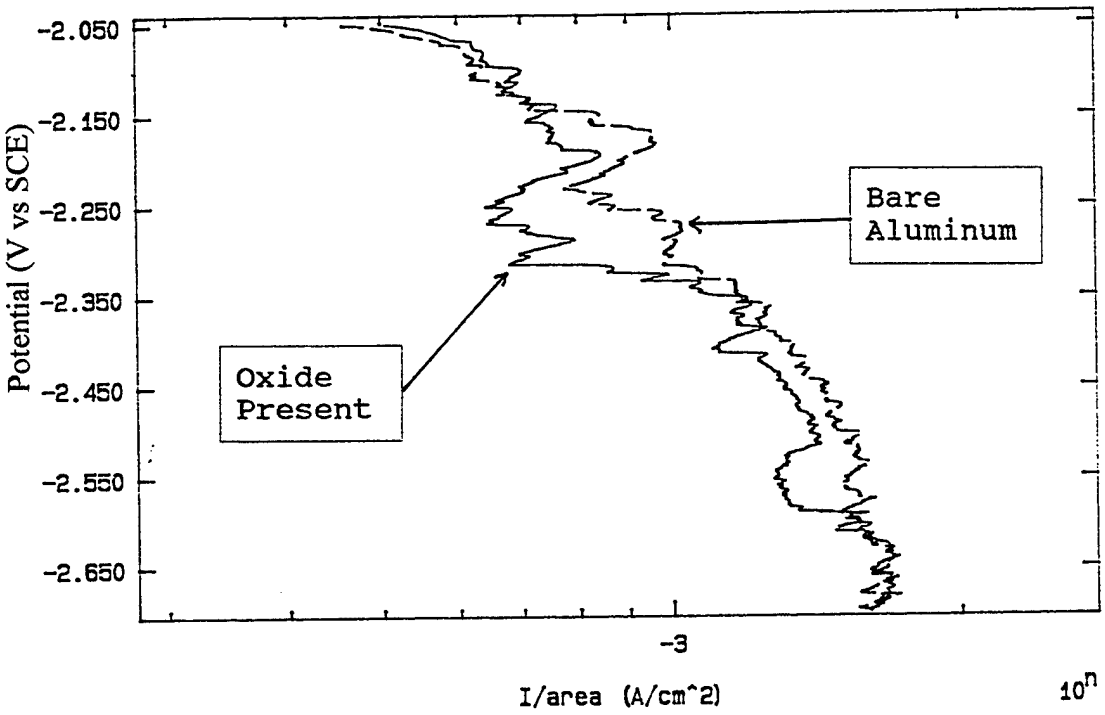

FIGURE 25: Polarization curves on the (100) single crystal for the oxide and bare aluminum case used in the hydrochloric acid experiment.

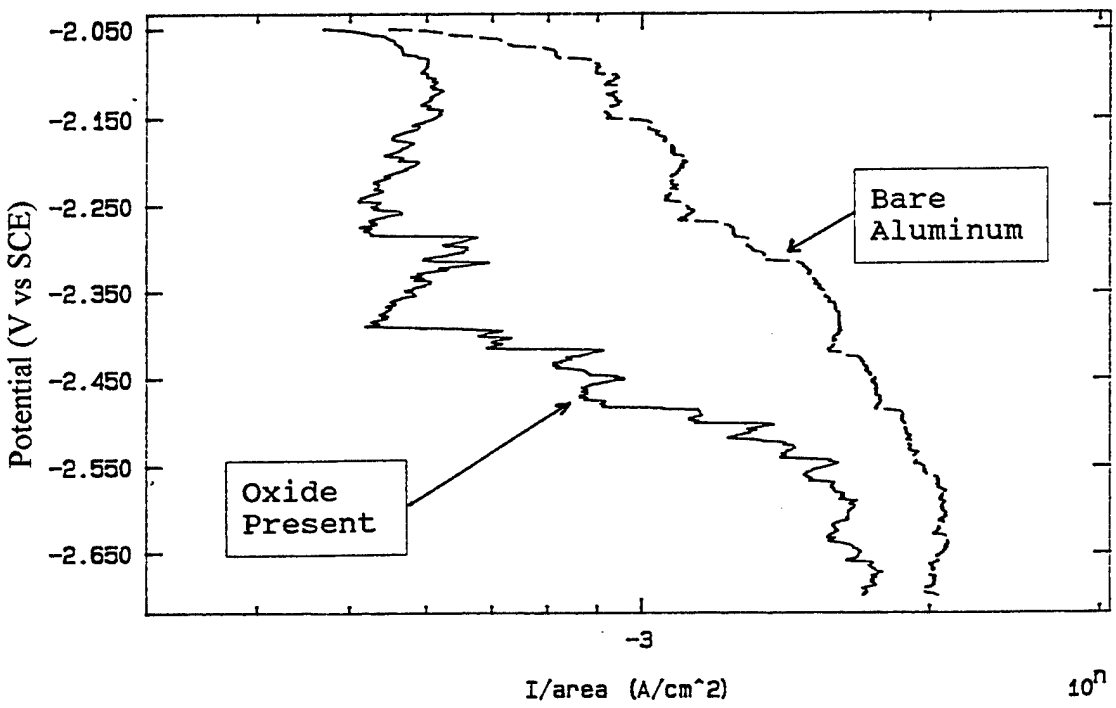

FIGURE 26: Polarization curves on the (110) single crystal for the oxide and bare aluminum case used in the hydrochloric acid experiment.

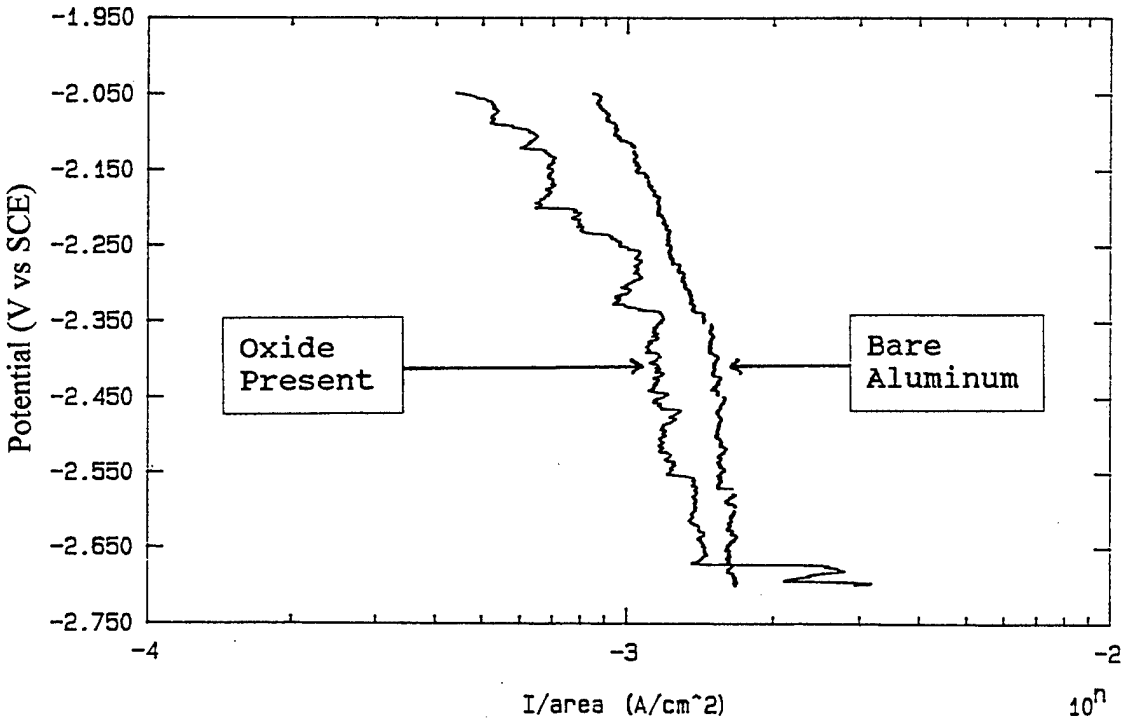

FIGURE 27: Polarization curves on the (111) single crystal for the oxide and bare aluminum case used in the hydrochloric acid experiment.

than the aluminum with an oxide layer. If the inside of a pit is oxide free, then the cathodic kinetics difference can be used to represent the cathodic reaction within the pit for metastable pitting and also for stable pitting.

A comparison of the potentiodynamic scans of the three crystal orientations with the oxide layer present showed that the (110) crystal had slightly lower cathodic kinetics, relative to the (111) and (100) crystals, which were about the same (Figure 28). Because the (100) and (111) curves were approximately the same, the results showed no obvious crystallographic dependence for the cathodic kinetics.

In contrast, a comparison of the potentiodynamic scans of the three orientations with a portion of the oxide removed, showed a dependence on the crystal orientation for the cathodic kinetics (Figure 29). The (100) crystal had the least active kinetics, while the (111) crystal had the most active kinetics. This relationship is in agreement with the other experimental results that showed that the (111) crystal was the most active orientation. The results also showed that on an oxide-free surface the order of the cathodic kinetics from most active to least active would be: (111), (110), (100).

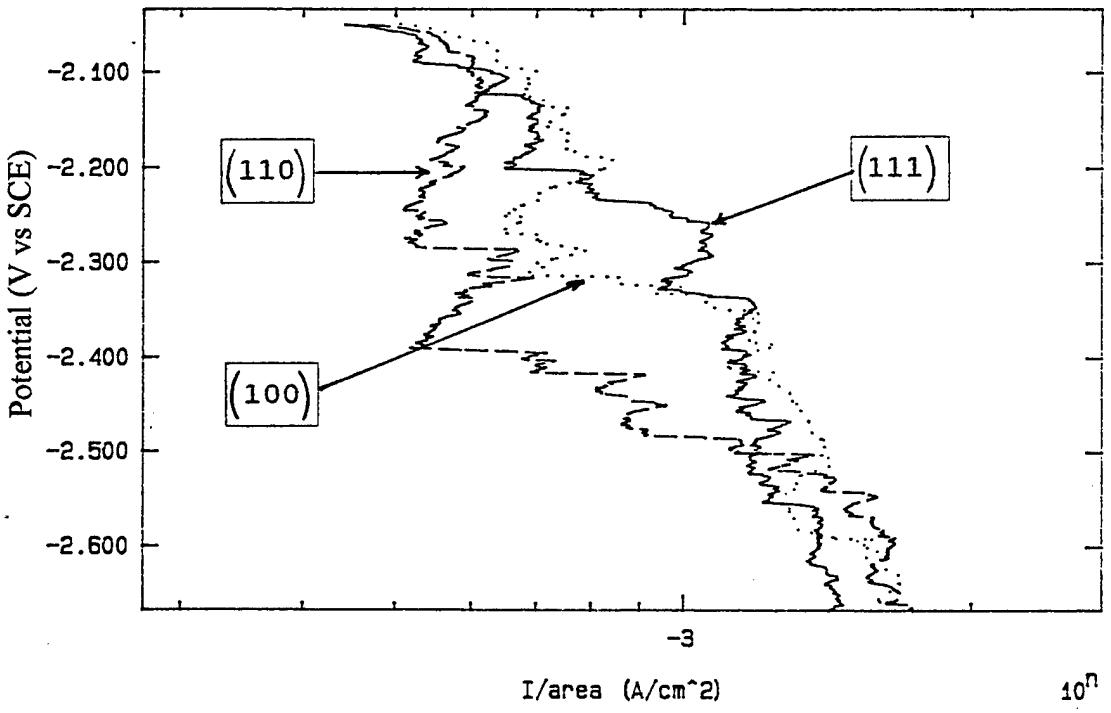

FIGURE 28: Polarization curves on the (100), (110), and (111) single crystals for the oxide present case used in the hydrochloric acid experiment.

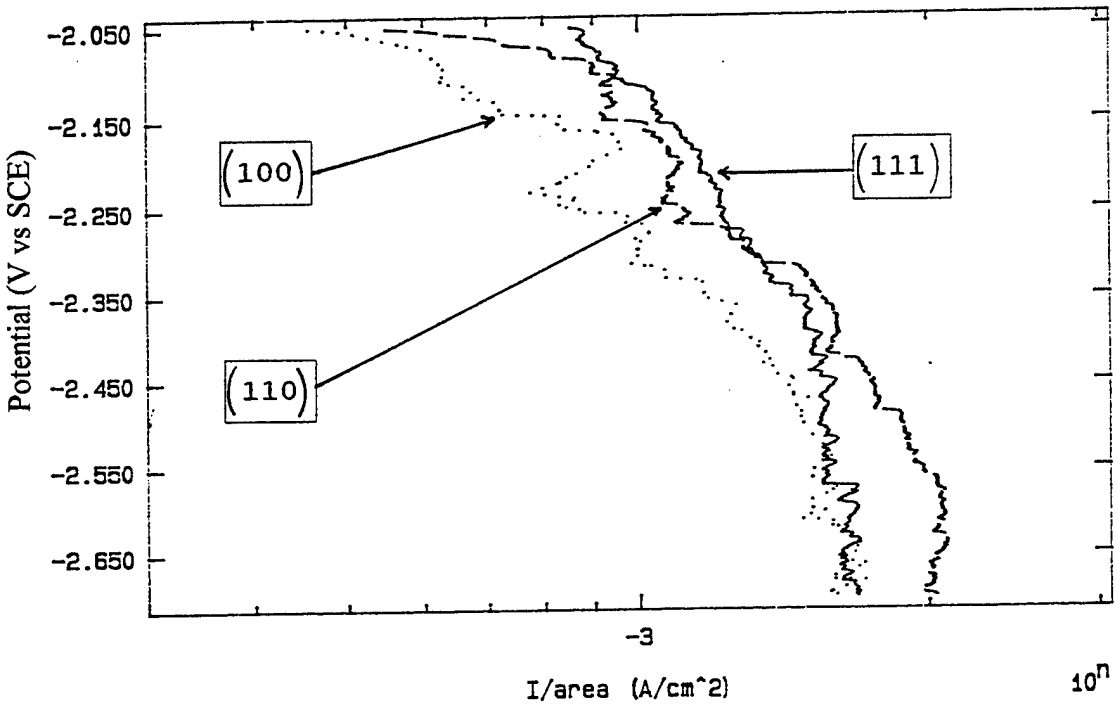

FIGURE 29: Polarization curves on the (100), (110), and (111) single crystals for the bare aluminum case used in the hydrochloric acid experiment.

The experiment in which 40 potentiodynamic scans were conducted on the (111) single crystal showed that time had a minimal effect on the cathodic kinetics of the aluminum crystal. As seen in Figure 30, there was little change between the potentiodynamic curves. The small amount of change that occurred did so in two steps. The first step included the first 15 potentiodynamic scans. During this step, the cathodic kinetics gradually becoming more active. The second step included the last 25 potentiodynamic scans. During this step the cathodic kinetics became less active; almost to the point where they matched the first potentiodynamic scan.

The potentiodynamic scan that produced both the cathodic and anodic kinetics showed that the corrosion potential of the (111) single crystal in the acidic solution was approximately -600 mV vs SCE (Figure 31). The scan also showed that the aluminum crystal exhibited no passivity, but rather active corrosion, in the anodic portion of the curve (above Ecorr). This is important because it showed the potential at which anodic dissolution occurred and indicated the approximate potential of the exposed faces within the pits. Additionally, the cathodic kinetics that would occur

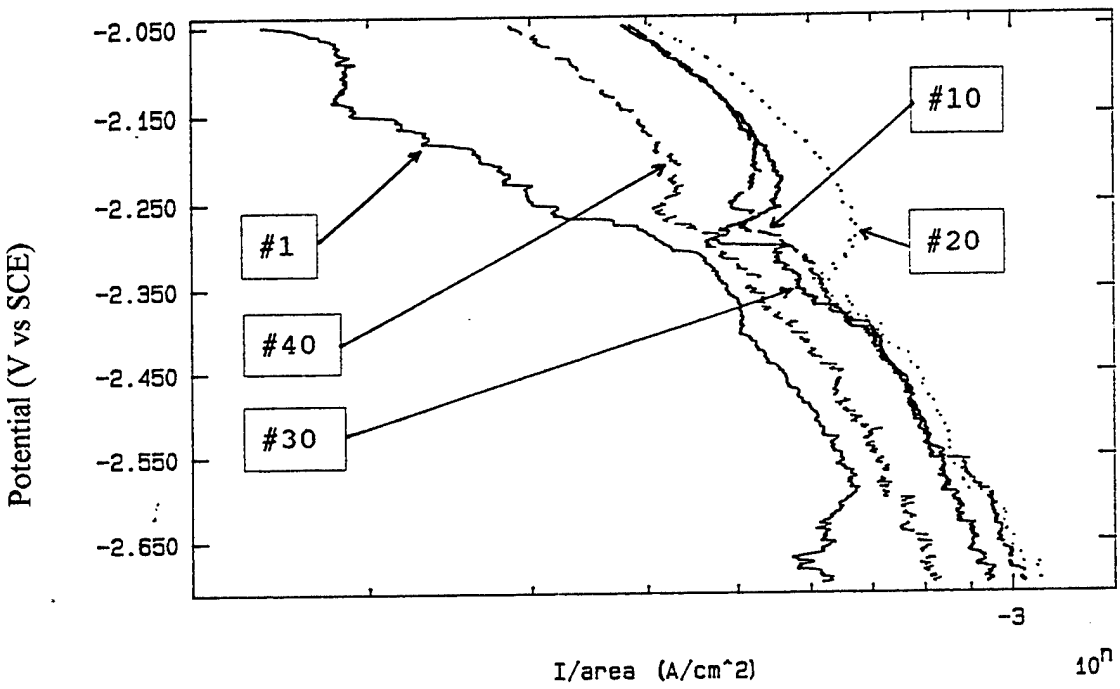

FIGURE 30: Polarization curves taken on a (111) single crystal in hydrochloric acid solution. These curves show the effect of time on the cathodic reaction rate of the aluminum crystal. The numbers listed above are the numbers of the polarization curves.

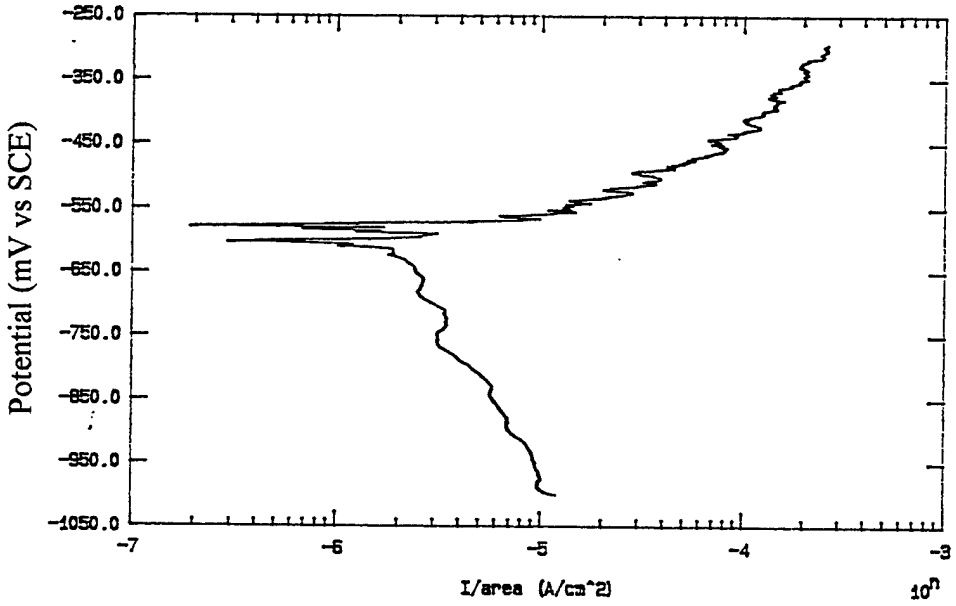

FIGURE 31: Polarization curve of a (111) single crystal. The corrosion potential was determined to be approximately -600mV vs SCE.

in the actual pitting process would be those at potentials near the Ecorr found in this test. Therefore, the three potentiodynamic scans can be extrapolated to the pitting potential to determine the influence of the crystal orientation on the cathodic kinetics at the most relevant potential (Figure 32). When the potentiostatic scans of the three single crystals, which were bared of oxide, were extrapolated to the pitting potential, it was found that the slope of the three potentiodynamic scans were not the same. The difference between the cathodic kinetics were accentuated with the (111) orientation having the fastest rate and the (100) orientation the slowest rate.

HYPOTHESIS ON THE ANISOTROPIC PITTING OF ALUMINUM

Experiments have shown that when aluminum pits, it pits crystallographically with the (100) faces being the resultant morphology [6,7]. This pitting morphology could be attributed to the rates of the corrosion reactions on each crystal face within the pit. If the rate of the corrosion reactions, either anodic or cathodic or both, were faster on one face than the rates of the reactions on another face, then this face would corrode faster until the

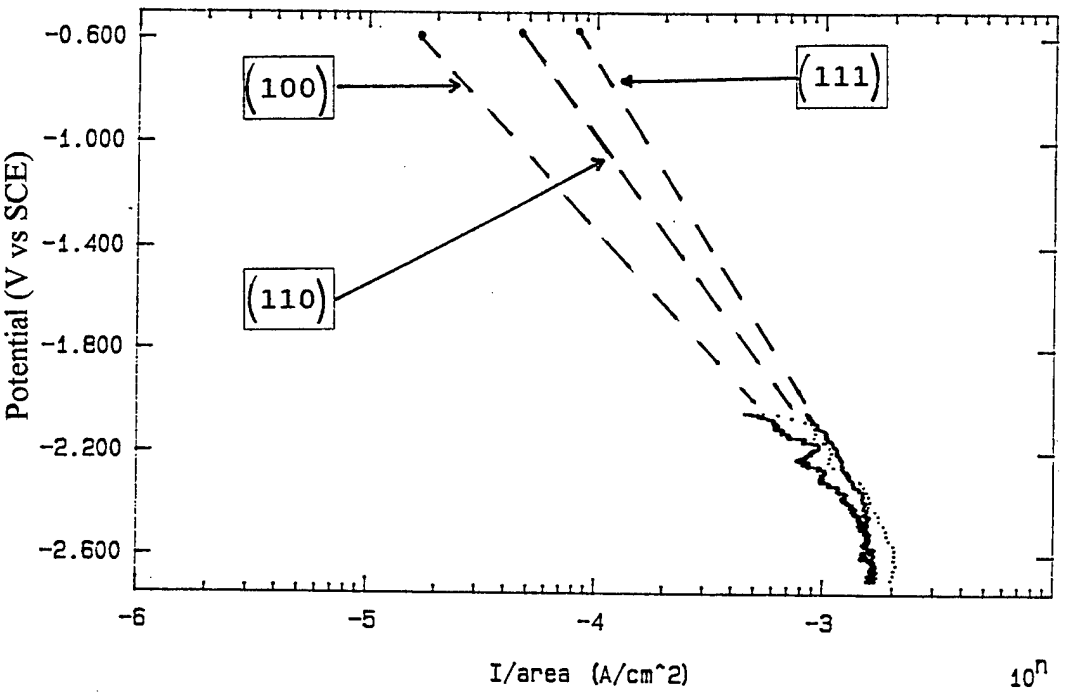

FIGURE 32: Polarization curves of (100), (110), and (111) single crystal in HCl extrapolated to the potential of the faces within a pit.

resultant morphology was dominated by the orientation with the slower reactions. Experimentally, the (100) orientation has been found to have slower reaction rates than the other two orientations. It is proposed that this is why the pitting of aluminum results in a strictly (100) orientation morphology.

Figure 33 shows a cross-section of a pit that has (100) and (110) orientations within it. This type of symmetry can be observed when looking into the crystal perpendicular to one of the unit cell faces. The dashed lines represent the progression of the facets within the pit as anodic dissolution (corrosion) occurs. If the (100) orientations have slower reaction rates, as proposed, then the dashed lines representing the (100) orientations would not move as quickly as the dashed lines representing the (110) orientations. As shown in the figure, the (110) orientations eventually corrode away to the point that they do not exist and the pit has a (100) oriented morphology. This argument can be extended to pits with (111) faces exposed since these have shown even faster reaction kinetics than the (110) faces.

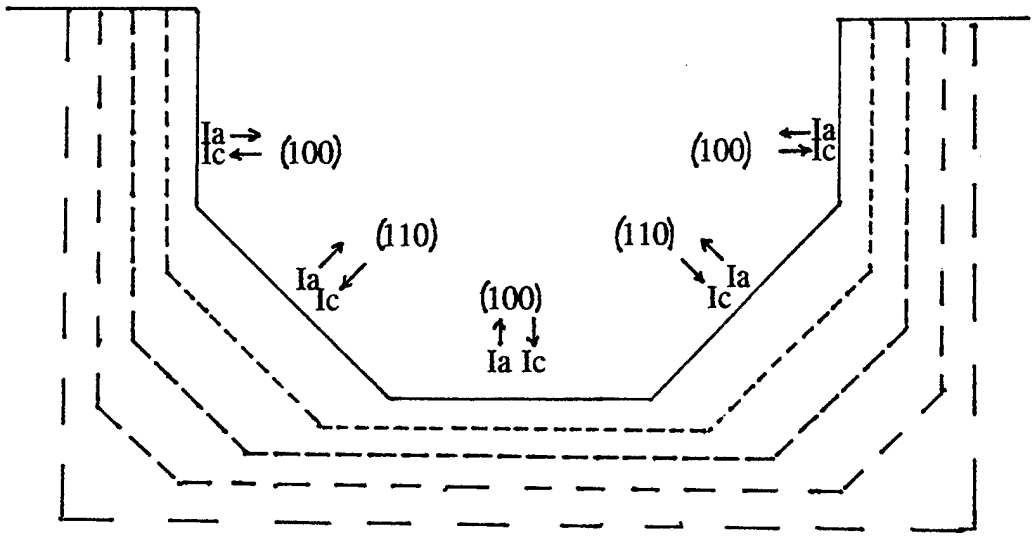

FIGURE 33: A cross section of a pit bounded by (100) and (110) orientations. The dashed lines represent the dissolution of the metal as a function of time. Ia and Ic represent the anodic and cathodic current densities respectively. The (110) orientation is corroding more than the (100) orientation, resulting in a (100) pit morphology.

CONCLUSIONS

The results of the metastable pitting experiments showed that the (111) single crystal orientation exhibited more metastable pitting than either the (100) or the (110) single crystal orientations as the potential neared the pitting potential of polycrystalline aluminum. This suggests that the (111) orientation initiates more readily than the other two orientations. Also, the results show that the (111) orientation undergoes an earlier transition to stable pitting than the other orientations. This suggests that this orientation maintains the stable pit chemistry more readily at the pitting potential of polycrystalline aluminum than the other orientations.

Pitting density examinations after the metastable experiments, as determined by current spikes and electron microscopy analysis, have shown that the pitting density is greater for the (111) orientation than the other two orientations. This suggests that the (111) orientation has a higher affinity for initiating and maintaining stable pit chemistry than do the other single crystal orientations.

On average, the peak pit currents for the (111)

orientation are higher than for the other two orientations. The results of the metastable experiments suggest that the rate of dissolution ($Al \rightarrow Al^{+3} + 3e^-$) is faster for the (111) orientation than the other orientations.

Two of the three Ecorr experiments showed that the passive film on the (111) orientation had more active cathodic kinetics than the other two orientations. The passive film on the (100) crystal was found to have the most inert cathodic kinetics for these same two experiments. The last Ecorr experiment contradicted these results. It is not understood why this contradiction occurred.

The hydrochloric acid experiments showed that the cathodic kinetics on bare aluminum are more active than on aluminum with an oxide film. Also, the results showed that the cathodic kinetics on bare aluminum at the potentials evaluated was in the following activity order: (111)>(110)>(100). When the cathodic reaction curves were extrapolated to the potential that would occur on the exposed faces within pits, the activity order remained the same and the difference between the orientations increased.

The (100) faceting of aluminum when it pits is a result of the difference in the rate of the anodic and cathodic

reactions for the orientations. Once the pit is formed and the dissolution begins, the (110) and (111) orientations corrode faster than the (100) orientation. The result of this difference in corrosion rate is that the (100) orientation becomes the dominant orientation within the pit.

ACKNOWLEDGMENTS

I would like to gratefully acknowledge Professor Patrick Moran for his guidance and patience during this project. I would also like to thank Dr. Paul Natishan from the Naval Research Laboratory for his guidance and help and for supplying the aluminum samples and other supplies. I would like to thank the lab technicians, Butch Antenucci and Steve Crutchley, for their help with the mechanics and setup of the project. I would also like to thank the Naval Research Laboratory for allowing me to use their facilities. I would also like to thank the NRL-USNA Cooperative Research Program, the Trident Scholar Research Program, and the USNA Mechanical Engineering Department for funding this project.

REFERENCES

1. Orem, T.H., Journal of Research of the National Bureau of Standards, **58**, 157 (1957).

2. Bargeron, C.B., Givens, R.B., National Association of Corrosion Engineers, **36**, 618 (1980)

3. Pride, S.T., Scully, J.R., Hudson, J.L., Journal Electrochemical Society, **141**, 3028 (1994).

4. Pryor, M.J., National Association of Corrosion Engineers, "Localized Corrosion", **3**, 2 (1971).

5. Scully, J.R., Pride, S.T., Scully, H.S., Hudson, J.L., Electrochemical Society Proceedings, **95-15**, 15 (1995).

6. Santarini, G., Boos, J.Y., Scripta Metallurgical, **8**, 1121 (1974).

7. Arora, O.P., Metzger, M., Microstructure and Corrosion, "Corrosion Anisotropy In Aluminum", 435 (1970).

8. Yasuda, M., Weinberg, Tromans, D., Journal Electrochemical Society, **137**, 3708 (1990).

9. Jones, D.A., Principles and Prevention of Corrosion, Prentice Hall Company, Upper Saddle River NJ., (1996).

10. Natishan, P.M., Peace, G.T., Slebodnick, P.F., Metallography, **23**, 21 (1989).

11. Diggle, J.W., Vijh, A.K., Oxides and Oxide Films, Marcel Dekker Company, New York, New York, (1976).